Norges miljø- og biovitenskapelige universitet

Master's Thesis 2021 30 ECTS

Faculty of Science and Technology

Development of Gas Composition Sensing Based on Acoustic Attenuation

Sander Wittwer

Mechanical Engineering and Process Technology

Preface

This thesis is the result of a master project in sensor technology and signal processing at the Norwegian University of Life Sciences (NMBU) Faculty of science and Technology (RealTek). It marks the end of a five-year Master of Science in Mechanical engineering and Process Technology. During the years at NMBU my interest and knowledge for machine learning and analytics as a tool for advanced signal processing has increased exponentially, and it was therefore a great privilege to be able to write a thesis within this topic.

During my time as a student I've been fortunate to have been a part of Eik Ideverksted. They have helped me learn beyond the curriculum offered by NMBU, and introduced me to interesting projects and partners. I am thankful to Disruptive Engineering and HSO, both for hiring me before the completion of my degree, and for being flexible during the writing of this thesis. I look forward to continuing working with them and my colleagues.

I would like to thank my supervisor Kristian Omberg, along with Odd Ivar Lekang for feedback and guidance.

Further, I also thank Ola Omberg for helping me build the chamber and transducer fittings used in the experiments and giving valuable feedback on the thesis.

Finally, I would thank everyone who helped me read through the thesis and correct my spelling mistakes.

Abstract

Usage of sensing technology has increased rapidly for the last decade. Measurements of gas concentrations can are used in a wide variety of areas like medical applications, monitoring in wastewater plants and air quality monitoring. The use of gas sensors is critical to plan and perform regular maintenance. It will in the near future provide a basis for improved predictive maintenance that uses data to detect anomalies and possible defects in equipment.

Currently, the gas sensor market is dominated by expensive optical or electrochemical sensors with low selectivity. Therefore, a focus has been on developing new cost-efficient technology that can counter the current limitations of the existing sensing technologies.

Better understanding of the physical principles behind attenuation of sound waves allows new sensing technology to be developed from traditional piezoelectric ultrasonic transducers. Attenuation of ultrasonic signals cause reduced kinetic energy as the sound wave travels in time. This is caused by friction, heat conduction, diffusion, and acoustic molecular relaxation for some gas mixtures in a certain specific frequency range.

Recent development in understanding of the acoustic molecular relaxation allows improved theoretical models for predicting acoustic attenuation and speed of sound in a wide variety of gas mixtures. In conjunction with the recent developments the interest in solving the reverse problem has increased which consists of using the attenuation of sound waves to predict gas compositions. This would allow a new generation of inexpensive, simple and robust gas sensing devices to be developed.

This thesis describes a method for determining the gas concentration based on acoustic attenuation. This is achieved using ultrasonic transducers operating at different frequencies. Machine learning is used on the transducer signals to detect and predict the gas concentration. In order to achieve this the following objectives for this work has been set:

- Research and review of theoretical work - investigation of the nonlinear behavior of the acoustic attenuation in mixtures of increasing CO_2 concentration.
- Technical review of existing acoustic attenuation models.
- Development of a theoretical method for predicting attenuation and speed of sound in gas mixtures.
- Obtain experimental attenuation data for nitrogen and carbon dioxide mixtures.
- Create a method for calculating attenuation and speed of the ultrasonic signals.

- Development and evaluation of predictive models using machine learning to predict the composition of carbon dioxide in nitrogen based on experimental data.
- Evaluate the algorithms and suggest a final model used for composition detection.
- Suggest further work to improve the concept.

Using a self developed experimental test rig fitted with off- the shelf transducers, and a range of pre-mixed N2—CO2 gas mixtures a set of ultrasound burst signals is created and measured. These measurements were verified using an identified theoretical model based on recent work on acoustic relaxation effects in attenuation of ultrasonic signals. Based on experimental data, machine learning was used to provide a final model which predicts the concentration of carbon dioxide. It performs with an average error of 0.7% (absolute CO2 mole fraction), the error is expected to be below 0.5% in mixtures with less than 20% carbon dioxide. This is an improvement compared to recent studies where the applied theoretical models gave errors above 2.4%.

The method developed in this work is transferable to applications like moderate carbon dioxide monitoring in exposed areas like mines or similar where high carbon dioxide levels might cause direct harm. In addition, it represents a possible method of reducing the complexity of the current sensor designs by focusing on intelligent signal processing in combination with simple transducers.

The results in this thesis show that further work on the concept could enable composition detection in mixtures of many gas components.

Sammendrag

Bruk av sensorteknologi har økt raskt det siste tiåret. Måling av gasskonsentrasjoner blir brukt i mange forskjellige områder som medisinske applikasjoner, overvåking av avløpsanlegg og luftkvalitetsovervåking. Gassensorer er avgjørende for å planlegge og utføre regelmessig vedlikehold, og vil i nær fremtid gi grunnlag for forbedret prediktivt vedlikehold som bruker data for å oppdage avvik og mulige feil i utstyr.

For tiden domineres markedet for gassensorer av dyre optiske eller elektrokjemiske sensorer med lav selektivitet. Derfor har det vært et økt fokus på å utvikle ny og kostnadseffektiv teknologi som kan overgå begrensningene med dagens eksisterende sensorteknologier.

Bedre forståelse av de fysiske prinsippene bak demping av lydbølger gjør det mulig for ny sensorteknologi å utvikles fra tradisjonelle piezoelektriske ultralydtransdusere. Demping av ultralydsignaler er forårsaket av friksjon, varmeledning, diffusjon, og akustisk molekylær relaksasjon for noen gassblandinger i bestemte frekvenser.

Nylig utvikling i forståelsen av akustisk relaksasjon tillater bedre teoretiske modeller for å forutsi akustisk demping og hastigheten til lydbølger i et bredt spekter av gassblandinger. I forbindelse med denne utviklingen har interessen for å løse det omvendte problemet økt, som består av å bruke dempning av lydbølger for å forutsi gassammensetninger. Dette vil tillate utvikling av en ny generasjon billige, enkle og robuste gassensorer.

Denne oppgaven beskriver en metode for å bestemme gasskonsentrasjoner basert på demping av lydbølger. Det oppnås ved bruk av ultralydtransdusere som opererer med forskjellige frekvenser. Maskinlæring blir deretter brukt på data fra transduserne for å oppdage og forutsi gasskonsentrasjoner. For å oppnå dette er følgende mål for arbeidet satt:

- Gjennomgang av teoretisk bakgrunn - forståelse av ulineariteten ved lyddemping i blandinger med økende konsentrasjon av CO_2.
- Gjennomgang av eksisterende modeller for å predikere akustisk demping.
- Utvikling av en modell for å predikere akustisk demping og lydens hastighet i gitte gassblandinger.
- Skaffe eksperimentell data for gassblandinger av nitrogen og karbondioksid.
- Utvikle en metode for å beregne demping og hastigheten til ultralydsignalene.
- Utvikle og evaluere prediktive modeller som bruker maskinlæring til å forutsi konsentrasjonen av karbondioksid i gassblandingene basert på den eksperimentelle dataen.

- Evaluere algoritmene og foreslå en endelig modell for å detektere gasskonsentrasjon.
- Foreslå videre arbeid for å forbedre konseptet.

Ved hjelp av en egenutviklet eksperimentell testrigg utstyrt med ultralydtransdusere og en rekke forhåndsblandede gassblandinger av nitrogen og karbondioksid ble et sett med eksperimentelle ultralydsignaler generert og målt. Disse målingene ble verifisert ved hjelp av en teoretisk modell basert på nylig arbeid med akustisk relaksasjon og demping av lyd. Basert på den eksperimentelle dataen ble maskinlæring brukt til å gi en modell som predikerer konsentrasjonen av karbondioksid i gassblandingene. Modellen har en gjennomsnittlig feil på 0,7% absolutt CO_2 molfraksjon, feilen forventes å være under 0,5% i blandinger med mindre enn 20% karbondioksid. Dette er en forbedring sammenlignet med nyere studier der de anvendte teoretiske modellene ga snittfeil på over 2,4%.

Metoden utviklet i dette arbeidet kan overføres til applikasjoner som moderat karbondioksidovervåking i eksponerte områder som gruver eller lignende der høye karbondioksidnivåer kan forårsake direkte skade. I tillegg representerer det en mulig metode for å redusere kompleksiteten til eksisterende sensorsystemer ved å fokusere på intelligent signalbehandling i kombinasjon med enkle transdusere.

Resultatene i dette arbeidet viser at videre arbeid med konseptet kan muliggjøre gassdeteksjon i et bredt spekter av gasser.

Contents

Contents i

List of Figures iv

List of Tables v

List of Abbreviations vi

1 Introduction 1
- 1.1 Problem Statement . . . 2
- 1.2 Goals and Objectives . . . 2
  - 1.2.1 Research and Review of Theoretical Work . . . 2
  - 1.2.2 Obtain Experimental Data . . . 2
  - 1.2.3 Development and Evaluation of Predictive Models . . . 3
- 1.3 Limitations . . . 3

2 Theory 4
- 2.1 Gases and Mixtures . . . 4
  - 2.1.1 Properties . . . 4
- 2.2 Ultrasound . . . 4
  - 2.2.1 Ultrasonic Transducers . . . 4
- 2.3 Speed of Sound . . . 5
- 2.4 Acoustic Attenuation . . . 5
  - 2.4.1 Absorption coefficient . . . 5
  - 2.4.2 Classical Attenuation . . . 6
- 2.5 Molecular Relaxation . . . 7
  - 2.5.1 Effect on Specific Heat . . . 8
  - 2.5.2 Attenuation Spectra . . . 9
  - 2.5.3 Single Relaxation Process . . . 9
  - 2.5.4 Multimode Relaxation Processes . . . 9
  - 2.5.5 Modes of Vibration . . . 10
- 2.6 Model for Attenuation and Speed of Sound . . . 12
- 2.7 Machine Learning . . . 14
  - 2.7.1 Regression . . . 14
  - 2.7.2 Neural Networks . . . 15
  - 2.7.3 Preprocessing and Training Techniques . . . 15
  - 2.7.4 Evaluation . . . 16

3 Review of Related Work **18**
3.1 Ultrasonic Sensing . . . 18
3.1.1 Attenuation Based Detection . . . 18
3.2 Sensing Based on Relaxation Models . . . 18
3.2.1 Reconstruction Algorithms . . . 18
3.2.2 Classification of Mixtures Based on GARAS . . . 19
3.2.3 Detecting Inflection Point of Frequency-dependent Velocity . 19
3.2.4 Concentration Measurements from Mixtures of CO_2 and N_2 20

4 Method **21**
4.1 Experimental Test Rig . . . 22
4.1.1 Equipment . . . 22
4.1.2 Chamber . . . 23
4.1.3 Transducers . . . 23
4.1.4 Characterization of Transducers . . . 24
4.2 Data Acquisition . . . 25
4.2.1 Gas Compositions . . . 25
4.2.2 Estimation of Experimental Parameters . . . 25
4.2.3 Acquiring Signals . . . 26
4.3 Preprocessing . . . 27
4.3.1 Filtering of Signals . . . 27
4.3.2 Calculating Attenuation of Signals . . . 29
4.3.3 Noise Detection . . . 30
4.3.4 Transformation of Raw Signals . . . 32
4.4 Estimation of Speed of Sound . . . 33
4.4.1 Cross Correlation . . . 34
4.4.2 Peak to Peak . . . 35
4.4.3 Threshold . . . 35
4.4.4 Evaluation . . . 35
4.5 Predictive Models . . . 36
4.5.1 Dataset Creation . . . 36
4.5.2 Support Vector Machine Regression . . . 37
4.5.3 Calibration of the Support Vector Machine . . . 38
4.5.4 Convolutional Neural Network . . . 40

5 Results and Discussion **43**
5.1 Analysis of the Sample Signals . . . 43
5.1.1 Echoes . . . 43
5.1.2 Conclusion of Signal Quality . . . 44
5.2 Comparison with Theoretical Model . . . 44
5.2.1 Attenuation . . . 45
5.2.2 Speed of Sound . . . 46
5.3 Comparison of the Predictive Models . . . 47
5.3.1 Final Model . . . 48

5.3.2 Comparison with Related Work 49
5.4 Problems and Uncertainties with Experimental Testing 49

6 Conclusion **50**
6.1 Summary 50
6.2 Further Work 50
6.2.1 Improving the Experimental Data 50
6.2.2 Improving the Models 51
6.2.3 Extended Analysis 51

Bibliography **52**

A Data Acquisition Protocol **56**
A.1 Objectives 56
A.2 Determination of test parameters 56
A.3 Setup 56
A.4 Procedure 57

B Transducer Characteristics **58**
B.1 Equivalent Circuit: 58
B.2 Characteristics 58

C Sample Signal Responses **59**
C.1 Tx1 59
C.2 Tx2 60
C.3 Tx3 61
C.4 Tx4 62
C.5 Tx5 63
C.6 Tx6 64
C.7 Tx7 65

List of Figures

2.1 Attenuation of a sound wave 6
2.2 Single relaxation process 7
2.3 Attenuation of soundwaves in N_2 and CO_2 11
2.4 Speed of sound for carbon-dioxide 12
2.5 Amplitude simulation 13
2.6 Speed of sound simulation 13

4.1 Model diagram 21
4.2 Principal test rig chart 22
4.3 Test rig - Picture 23
4.4 Transducer equivalent circuit 24
4.5 Filtered signal with forward-reverse filtering 28
4.6 Comparison of unfiltered and filtered signal (Tx4) 28
4.7 Boxplot of the transducers initial amplitudes 30
4.8 SNR samples 31
4.9 SNR decay function 32
4.10 Logarithmic transformation of raw signals 33
4.11 Prediction flowchart 36
4.12 Result for the SVM 38
4.13 Residual plot from the SVR model 38
4.14 Calibration of SVM 39
4.15 Calibration results of SVM 40
4.16 Result for the CNN 41
4.17 Residual plot from the CNN model 41

5.1 Echo in nitrogen using Tx7 (100kHz) 43
5.2 Comparison of echoes in Tx6 44
5.3 Results - Attenuation 45
5.4 Results - Amplitude 46
5.5 Result - Speed of sound 47

C.1 Filtered signal samples in Tx1 59
C.2 Filtered signal samples in Tx2 60
C.3 Filtered signal samples in Tx3 61
C.4 Filtered signal samples in Tx4 62
C.5 Filtered signal samples in Tx5 63
C.6 Filtered signal samples in Tx6 64
C.7 Filtered signal samples in Tx7 65

List of Tables

2.1 Properties of relevant gases at 300K 4
2.2 Vibrational modes for nitrogen and carbon-dioxide at 300K 11

4.1 List of transducers and relevant parameters 23
4.2 Transducer characteristics 25
4.3 Gas compositions for the experiments 25
4.4 Experimental parameters 26
4.5 Initial amplitudes for the transducers 29
4.6 Samples in the dataset 37
4.7 SVM - Optimal parameters 37
4.8 CNN Architecture 40

5.1 Mean relative errors for the experimental attenuations (α) 46
5.2 Mean relative errors for the estimated speed of sound 47
5.3 Results from the various models 48
5.4 Error estimations for the final predictive model 48

List of Abbreviations

MOS	Metal-Oxide Semiconductor
DOF	Degree Of Freedom
IMH	Isochoric Molar Heat
SVM	Support Vector Machine
RBF	Radial Basis Function
CNN	Convolutional Neural Network
MRA	Multi Resolution Analysis
IIR	Infinite Impulse Response
SNR	Signal to Noise Ratio
LTI	Linear Time Invariant
TDE	Time Delay Estimation
GCC	Generalized Cross-Correlator
IQR	Interquartile Range
MAE	Mean Absolute Error
MSE	Mean Squared Error
RMSE	Root Mean Squared Error

1. Introduction

In a quest to empower our ability to perceive our surroundings in new ways and provide end-users with improved data driven decisions the use intelligent sensing technology has exponentially increased during the previous decade.

One such sensing technology that is experiencing a surge in popularity is the measurements of concentration of a certain gas in an operational environment such as chemical industry, monitoring in wastewater plants, medical applications and environmental air quality monitoring [1]. For example air quality monitoring; The World Health Organization (WHO) estimates that poor air quality is linked to about 6.5 million deaths each year and the global health and welfare losses in 2013 were valuated at $5.1 trillion [2]. By employing air quality sensors one can enable the end user to make informed decisions that can help reduce the amount of air pollution in an urban area or at a workplace.

Another industrial demanding application is condition monitoring of industrial equipment that use gaseous dielectric mediums for high-voltage circuit breakers, switchgear and other electrical equipment, often replacing oil filled circuit breakers (OCBs). Leakage of these dielectric mediums can cause significant emissions of potent climate gases like SF6 [3]. The use of gas sensors is critical to plan and preform regularly maintenance and will in the near future provide the basis for an improved predictive maintenance that uses data to detect anomalies and possible defects in equipment [1].

Currently, the gas sensor market is dominated by expensive optical sensors or electrochemical sensors with low selectivity like Metal-Oxide Semiconductor (MOS). These solutions tend to become increasingly expensive depending on the application. This is caused by an increased complexity using advanced materials to increase sensitivity in addition to complex signal processing often resulting in a limited lifespan [4]. Therefore, a focus has been on developing new cost-efficient technology that can counter the current limitations of the existing sensing technologies.

Recent development in understanding of the acoustic molecular relaxation allows theoretical models for predicting acoustic attenuation and the related speed of sound in a wide variety of gases and gas mixtures. In conjunction with the recent developments the interest in solving the reverse problem has increased, which consists of using the attenuation of sound waves to predict gas compositions. This would allow a new generation of inexpensive, simple and robust gas sensing devices to be developed.

This thesis describes a method for determining the gas concentration based on acoustic attenuation. This is achieved using ultrasonic transducers operating at different frequencies. Machine learning is used on the transducer signals to detect and predict the gas concentration.

The method proposed here can be used for moderate gas concentration measurements of carbon dioxide or similar. Another thought application of ultrasonic

sensors is anomaly detection which can be applied when the gas composition is not expected to change over time. This can be used in smoke detectors and other alerting systems.

1.1 Problem Statement

The main purpose of this work is to investigate how ultrasonic signals are affected by the gas it is travelling in, and how the attenuation and speed of sound can be used for predicting and monitoring gas compositions. This will be accomplished using ultrasonic transducers operating at specific frequencies. The overall goal is to develop a method of predicting the gas composition in a system based on machine learning and ultrasonic signals.

1.2 Goals and Objectives

In order to achieve this the following objectives for this work has been set.

1.2.1 Research and Review of Theoretical Work

Investigation of the nonlinear behavior of the acoustic attenuation in mixtures of increasing CO_2 concentration.

- Identify key concepts and existing work.
- Obtain experimental data to be used for reference.
- Technical review of existing attenuation models.
- Suggest and develop a theoretical method for predicting attenuation and speed of sound in gas mixtures.

1.2.2 Obtain Experimental Data

The experimental data will be used for validation of the theoretical model and development of the gas composition sensing model. In order to do this the test rig needs to be able to transmit and receive ultrasonic signals at multiple frequencies.

An important part of this objective is to extract valuable information like attenuation and speed of sound. Only mixtures of nitrogen and carbon dioxide will be used for experiments due to limited time.

The main objectives here are:

- Create an experimental test rig for transmitting ultrasonic signals.
- Obtain experimental data.
- Create a method for calculating attenuation of the ultrasonic signals.

- Find and verify a method for calculating the speed of sound of the ultrasonic signals.

1.2.3 Development and Evaluation of Predictive Models

Machine learning will be used to predict the composition of carbon dioxide in nitrogen.

- Obtain relevant parameters from the experimental data to be used for composition prediction.
- Development of machine learning algorithms for predicting carbon dioxide concentration based on experimental data.
- Evaluate the algorithms and suggest a final model used for composition detection.

1.3 Limitations

Since the amount of required experimental work increases rapidly with the amount of gas compositions used the development of the models are limited to mixtures of nitrogen and carbon dioxide.

2. Theory

2.1 Gases and Mixtures

Most of the work here is done on binary gas mixtures which is a mixture consisting of two gas components. However, all theories are applicable to mixtures of more gas components

2.1.1 Properties

A set of common properties will be used for each gas. These include heat capacity, thermal conductivity and viscosity amongst others.

When mixing components the properties are multiplied with the mole fraction of each gas component, which should be close enough for approximations done in this work.

In table 2.1 relevant properties for used gases are listed. Viscosities are retrieved from the collection in *Viscosity of Gases* [5] and conductivities are retrieved from *Thermal Conductivity of Gases* [6]. Molar weights are retrieved from [7, 8].

Table 2.1: Properties of relevant gases at 300K

Gas	Viscosity $\eta/\mu\mathrm{Pa\,s}$	Conductivity $\kappa/\mathrm{mW\,m^{-1}\,K^{-1}}$	Molar Weight $M/\mathrm{kg\,mol^{-1}}$
Nitrogen	17.9	25.9	28.014
Carbon Dioxide	15.0	16.8	44.009

2.2 Ultrasound

Sound waves in gases occur when external forces acts on the gas causing pressure waves to travel through the medium. This causes elastic, pressurized oscillations where the amplitude of pressure is proportional to the particle displacements.

Ultrasonic sound is sound with frequencies higher than the human ear can hear. This occurs at frequencies larger than 20 kilohertz (kHz). There is no upper frequency limit, and frequencies up to multiple gigahertz (GHz) can be seen used in various applications [9, 10].

2.2.1 Ultrasonic Transducers

The ultrasonic transducer is an electronic device that generates ultrasound. Usually piezoelectric materials are used which converts electrical signals into the mechanical forces. Other transducers use moving electrical coils or conducting materials (EMAT).

For the transducers to work an external oscillating voltage is applied. The frequency of the oscillations should equal the frequency of the sound. Some frequencies give resonance on the materials which causes higher amplitudes, this frequency is often chosen as the frequency of the transducer. Although other frequencies can be applied as well these do not give as high sound amplitude and might not be detectable from distance [9].

The transducers can also be used as ultrasonic receivers [9]. In these cases the sound pressure induces an electric voltage on the circuit. This would normally only work at frequencies which corresponds to the transducers' resonance frequency. A transducer used as a receiver is often referenced to as a transceiver.

2.3 Speed of Sound

The speed of sound is the speed of the sonic pressure wave. In classic acoustics it is normally expressed as [11]:

$$c = \sqrt{\frac{\gamma RT}{M}} \tag{2.3.1}$$

where R is the universal gas constant ($R \approx 8.314 \frac{J}{mol \cdot K}$) [12], M is the molecular weight of the gas, T is the absolute gas temperature in kelvin and γ is the ratio of specific heats ($\gamma = \frac{C_p}{C_v}$).

For a mixture of gases the speed of sound is calculated as:

$$c_{mix} = \sqrt{\frac{\gamma_{mix} RT}{\sum_i [x_i M_i]}} \tag{2.3.2}$$

where γ_{mix} is the ratio of the specific heats for the mixture.

2.4 Acoustic Attenuation

As the ultrasonic waves travel trough a medium it is exposed to friction, heat conduction and diffusion, which causes attenuation of the sound wave [11, 13].

The Attenuation can be described with the amplitude exposed to an exponential decay [14, p. 38]:

$$A = A_0 e^{-\alpha z} \tag{2.4.1}$$

where A is the amplitude of pressure, A_0 is the initial amplitude, z is distance travelled and α is the absorption coefficient.

Figure 2.1 below illustrates how a sound wave travelling in a medium is gradually absorbed.

2.4.1 Absorption coefficient

The absorption coefficient (α) can be described by two parts:

$$\alpha = \alpha_c + \alpha_r \tag{2.4.2}$$

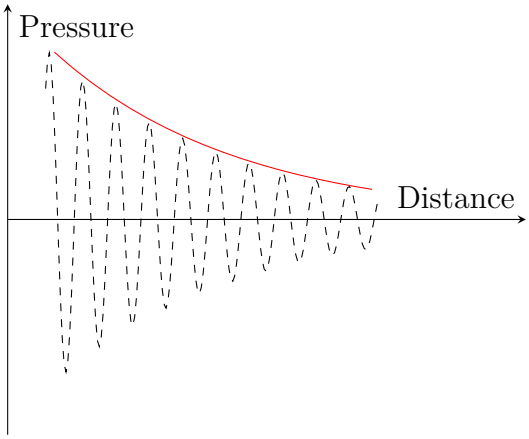

Figure 2.1: Illustration of how attenuation affects a sound wave. The red solid curve resembles the pressure for a single wave amplitude, and the dashed black line shows how the pressure is distributed over distance at a specific time for multiple sound waves.

where the subscripts indicate classical and relaxation, respectively. Classical attenuation is caused by absorption due to viscous losses from friction (as described by G.G Stokes). The attenuation caused by relaxation is the part which cannot be described with classical physics and stokes equation, and is caused by acoustic molecular relaxation, see section 2.5.

When describing relaxation a "dimensionless" variant of the absorption coefficient is often used, and is described as [15]:

$$\alpha\lambda = \alpha \cdot \frac{c}{f} \tag{2.4.3}$$

where λ is the wave-length, c is the speed of sound and f is the sound frequency.

2.4.2 Classical Attenuation

In classical physics attenuation of a sound waves is described by G. G. Stokes as a frequency-dependent value [11]. The following equation shows a generalized version which also takes thermal conductivity into account:

$$\alpha = \frac{\omega^2}{2\rho_0 c^3}\left(\frac{4}{3}\eta + (\gamma - 1)\frac{\kappa}{C_p}\right) \tag{2.4.4}$$

ω is the angular frequency of the wave, η is the dynamic viscosity of the gas mixture, ρ is the density of the gas mixture, γ is the ratio of specific heats, C_v, C_p are the specific heats respectively for constant volume and pressure, κ is the thermal conductivity of the mixture, and c is the speed of sound in the mixture.

As can be seen in eq. (2.4.4) the absorption factor grows quadratic with the frequency of sound. This causes high-frequent sound to be relatively short-lived.

2.5 Molecular Relaxation

Molecular relaxation occurs when the sound wave hits a molecule and the molecule excites to a new energy level. At this point energy captured by the excitation needs some time to be released (de-excitation). If the sound pressure wave passes before the energy is recaptured, the pressure wave loses more energy which causes absorption of the sound wave.

Sound waves moving in excitable gases will also be exposed to relaxation which causes absorption of wave energy. The excitation occurs when energy from molecular collisions is transformed to any internal Degree Of Freedom (DOF) in the molecules (excitation). For a sound wave, the transferred energy would lead to energy loss until de-excitation occurs. The time needed for reversing the adjustment in the DOF to a factor of e^{-1} is called the relaxation time τ [14, p. 56]. The energy loss increases with the sound frequency.

The dimensionless absorption factor for a single relaxation process is proportional to:

$$\frac{\omega\tau}{1+(\omega\tau)^2} \tag{2.5.1}$$

where ω is the angular frequency of the sound wave, and τ is the relaxation period. This expression has its maximum when $\omega\tau = 1$. The sound frequency at the pole can thereby be found at $f' = \frac{1}{2\pi\tau}$, where $f' = \frac{\omega}{2\pi}$ is the sound frequency. A sound wave is exposed to the particular relaxation process when its frequency approaches or exceeds f' [14].

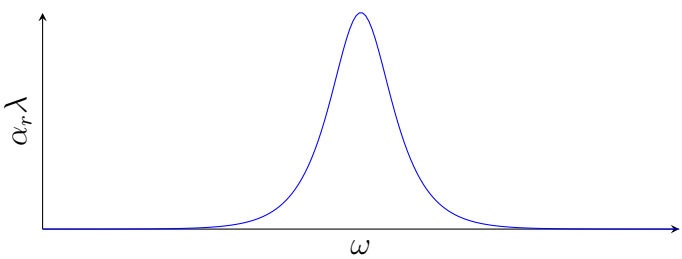

Figure 2.2: Change of absorption caused by a single relaxation process. The x-axis has a logarithmic scale.

There are three groups of DOFs: vibrational, translational, and rotational. Rotational adjustments only yield relatively small relaxation times. The effect caused by these are negligible for most gases at room temperature since the classical attenuation is fairly large when the sound frequency approaches higher frequencies [16].

For relaxation to be detectable it must occur at relatively low frequencies (below 1000kHz). At higher frequencies it can be assumed that the contribution of classical absorption is orders of magnitude larger and relaxation effects can therefore be hard to detect.

2.5.1 Effect on Specific Heat

In molecular relaxation study it has been found that the isochoric specific heat C_v is dependent on the state of the gas. When in an excited state the changes in speed and attenuation can be described by the change of the effective isochoric and isobar specific heats, $C_v^{eff}(\omega)$ and $C_p^{eff}(\omega)$ [13], ω is the angular frequency of the sound wave. Changes in the specific heat is expressed with the effective Isochoric Molar Heat (IMH), C_v^{vib}. For the effective specific heats, Mayer's relation holds for any state of the gas:

$$C_P^{eff}(\omega) - C_v^{eff}(\omega) = R \tag{2.5.2}$$

where $R = 8.314 \frac{\mathrm{J}}{\mathrm{mol\ K}}$ is the universal gas constant. And the effective specific heat ratio is:

$$\begin{aligned} \gamma^{eff}(\omega) &= \frac{C_p^{eff}(\omega)}{C_v^{eff}(\omega)} \\ &= \frac{C_v^{eff} + R}{C_v^{eff}(\omega)} \end{aligned} \tag{2.5.3}$$

The effective isochoric specific heat for a single degree of freedom can be found with the complex relation [14, p. 59]:

$$C_v^{eff}(\omega) = C_v^{\infty} + \frac{C^{int}}{1 + i\omega\tau} \tag{2.5.4}$$

where C_v^{∞} is the specific heat belonging to the external degree of freedom (external IMH), and equals the effective specific heat as the angular frequency approaches infinity:

$$C_v^{\infty} = \lim_{\omega \to \infty} C_v^{eff}(\omega) \tag{2.5.5}$$

The external IMH depends on molecular symmetry. For a linear molecule the external IMH is $C_v^{\infty} = 5R/2$, where R is the universal gas constant.

C^{int} is the internal specific heat which belongs to the corresponding degree of freedom:

$$C^{int} = C_v^0 - C_v^{\infty} \tag{2.5.6}$$

where C_v^0 is the specific heat at any static state:

$$C_v^0 = \lim_{\omega \to 0} C_v^{eff}(\omega) \tag{2.5.7}$$

Now looking at eqs. (2.3.1), (2.5.2) and (2.5.4) it is evident that the sound speed will change as the ratio of heats changes. High frequent waves cause a decrease in the effective isochoric heat capacity, then the heat capacity ratio $\gamma = \frac{C_P}{C_v}$ increases which leads to an increase in speed of sound.

Zhang, Wang, and Zhu used ultrasonic measurements to show how the frequency affects the speed of sound. They found that mixtures with CO_2 could have large speed variations from low to high frequencies [17].

2.5.2 Attenuation Spectra

The relaxation attenuation spectrum, often referenced to as GARAS (Gas Acoustic Attenuation Spectrum), shows the dimensionless absorption coefficient from relaxation at the given frequency spectrum.

The acoustic relaxation spectra is given with the relaxation part of the dimensionless absorption constant such that $\mu(\omega) = (\alpha_r \cdot \lambda)$. Therefore:

$$\mu(\omega) = \alpha_r \cdot \frac{c}{f} \tag{2.5.8}$$

$$\implies \alpha_r = \mu(\omega)\frac{f}{c} \tag{2.5.9}$$

2.5.3 Single Relaxation Process

A single relaxation process can be described in terms of the energy required for excitation and the relaxation time as [18]:

$$\begin{aligned} \mu_s(\omega) &= A_s C_v^{vib} \frac{\omega\tau}{1+(\omega\tau)^2} \\ A_s &= \frac{\pi R}{C_v^{\infty 2} + RC_v^{\infty} + C_v^{\infty} C_v^{vib} + \frac{1}{2} RC_v^{vib} + \frac{1}{2} C_v^{vib2}} \end{aligned} \tag{2.5.10}$$

2.5.4 Multimode Relaxation Processes

If only a single relaxation process exists, eq. (2.5.10) holds, and the dimensionless absorption is proportional to the equation. However, when multiple relaxation processes exist there are different theories on whether the relaxation shows up at the same time or not [14, p. 90]. Fundamental theories of relaxation is divided into two different theories, developed with different molecular energy transfer mechanisms.

Parallel theory assumes that each degree of freedom is vibrational, and excitation/de-excitation occurs in parallel [14, p. 93].

Series relaxation theory assumes excitations of the different degrees of freedom behaves like chemical reactions in series [14, p. 105].

Recent research shows that it is probably some combination of the two theories above [15, 18, 19].

Relaxation Model

The model developed by Zhang, Wang, Zhu, Ding, and Hu shows good results for gas mixtures where there are few dominant vibrational modes [15, 18]. This model will be used for reference and verification of the experiments in this work.

The effective heat capacity is found as:

$$C_v^{eff} = C_v^{\infty} + \sum_i^N \frac{C_i^{int}}{1+(i\omega\tau_i)^2} \tag{2.5.11}$$

where N is the total number of internal vibrational modes of the mixture, C_i^{int} is the contribution from the IMH for the specific vibrational mode and τ_i is the relaxation time. $C_v^{\infty} = \sum_l^W a_l C_{vl}^{\infty}$ is the external IMH, W is the number of molecules, C_{vl}^{∞} is the external IMH for the molecule and a_l is the mole fraction of the molecule.

C_i^{int} is calculated as the sum of the internal vibrational heat and mole fraction:

$$C_i^{int} = a_l C_i^{vib} \tag{2.5.12}$$

where a_l is the mole fraction of the corresponding molecule.

Taking the real part of C_v^{eff}, the acoustic spectra from eq. (2.5.10) becomes:

$$\begin{aligned} \mu_s(\omega) &= A_m \sum_i^N C_i^{int} \frac{\omega\tau_i}{1+(\omega\tau_i)^2} \\ A_m &= \frac{\pi R}{C_v^{\infty 2} + RC_v^{\infty} + C_v^{\infty}\sum_i^N C_i^{int} + \frac{1}{2}R\sum_i^N C_i^{int} + \frac{1}{2}(\sum_i^N C_i^{int})^2} \end{aligned} \tag{2.5.13}$$

The interior relaxation processes $\mu_i(\omega)$ are calculated as in eq. (2.5.10) replacing vibrational IMH with C_i^{int}:

$$\begin{aligned} \mu_i(\omega) &= A_i C_i^{vib} \frac{\omega\tau}{1+(\omega\tau)^2} \\ A_i &= \frac{\pi R}{C_v^{\infty 2} + RC_v^{\infty} + C_v^{\infty} C_i^{vib} + \frac{1}{2}RC_i^{vib} + \frac{1}{2}C_i^{vib2}} \end{aligned} \tag{2.5.14}$$

The multimode relaxation spectra $\mu_m(\omega)$ can be approximated taking the sum of the interior processes:

$$\mu_m(\omega) \approx \sum_i^N \mu_i(\omega) \tag{2.5.15}$$

2.5.5 Modes of Vibration

The number of vibrational modes for a gas depends on the molecule structure. Nitrogen only has translational stretching, while carbon-dioxide has four modes of vibration [20].

The related vibrational modes and relevant properties are shown in table 2.2. Note that the second mode of carbon-dioxide (v_2) includes two actual modes of bending which has the same wavelength. Relaxation times are from experimental results from Zhang, Wang, Zhu, Ding, and Hu [15].

Table 2.2: Vibrational modes for nitrogen and carbon-dioxide at 300K

Gas	Mode	Wavenumber/cm^{-1}	Type	C_V^{vib}/J mol^{-1} K^{-1}	τ/s
N_2	v_1	2331	Stretching	$1.38 \cdot 10^{-2}$	5.8
CO_2	v_1	1388	Sym. stretch	$4.73 \cdot 10^{-1}$	$1.45 \cdot 10^{-6}$
	v_2	677	Bending	7.53	$5.01 \cdot 10^{-6}$
	v_3	2349	Assym. stretc	$1.34 \cdot 10^{-2}$	$9.08 \cdot 10^{-2}$

As seen in table 2.2 the internal heat capacity of nitrogen is orders of magnitude lower than the internal heat capacity of the primary mode of carbon dioxide (v_2). Therefore, the relaxation strength caused by carbon dioxide is expected to cause significantly more attenuation of the sound waves.

Using table 2.2 and eqs. (2.4.1), (2.4.4) and (2.5.13) the absolute attenuation in nitrogen and carbon dioxide in fig. 2.1 is shown. For sound frequencies in the range between 10kHz and 600kHz relaxation is the major contributor to the attenuation.

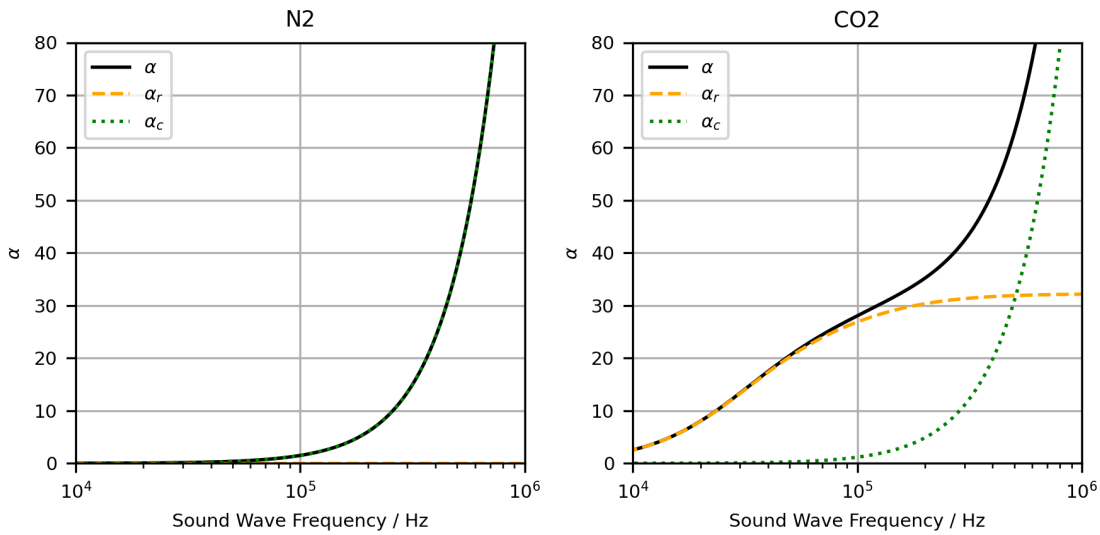

Figure 2.3: Attenuation of soundwaves in N_2 and CO_2. The solid black lines show the total attenuation α. The dashed orange lines show the attenuation caused by relaxation and the dotted green line show the classical attenuation.

In comparison, nitrogen shows no sign of relaxation at these frequencies due to low vibrational heat capacity and higher relaxation time τ.

Using data from table 2.2 the speed of sound for carbon-dioxide is shown in fig. 2.4. The inflection point is where the imaginary part has its maximum and corresponds to the point at $\omega\tau = 1$ for the primary relaxation mode (v_2), the non-significant modes, v_1 and v_3 gives negligible changes of the speed.

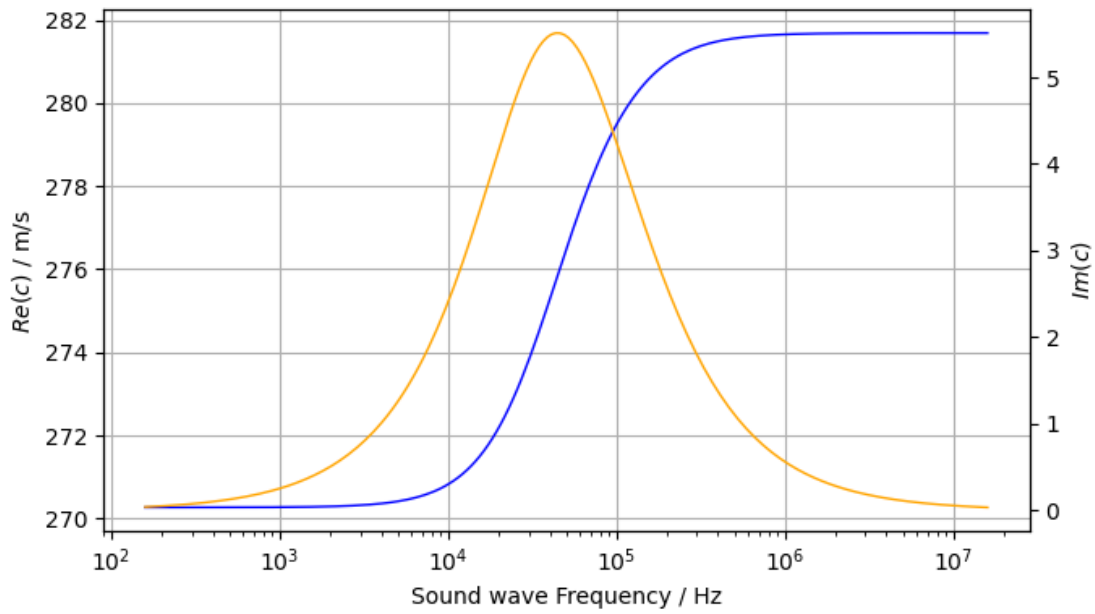

Figure 2.4: Speed of sound for carbon-dioxide. The real part is shown as the blue line on the left axis, and the imaginary part is the orange line on the right axis.

2.6 Model for Attenuation and Speed of Sound

The theoretical model from section 2.5.4 is used for calculating the molar heats and attenuation for the transducers.

Then the formulas for speed of sound and absorption is applied to create a simulation of the expected results. This is modeled using the python programming language.

The model is applied to mixtures of carbon dioxide and nitrogen. In fig. 2.5 below the relative amplitude A/A_0 is shown using three dimensional plots. The effects of relaxation can easily be seen as the amplitude shrinks for larger concentrations of carbon dioxide and high frequencies. The speed of sound in fig. 2.6 shows that the speed of sound behaves mostly linearly with concentration, except in mixtures with higher concentrations of carbon dioxide where it can be seen that the speed of sound is dependent on frequency, eg at 100% CO_2.

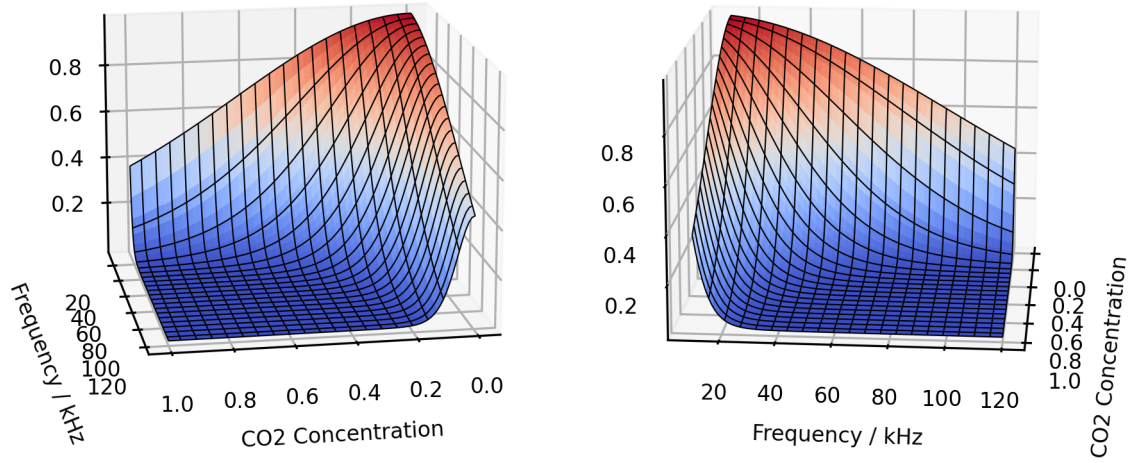

Figure 2.5: Surface plot of the simulated amplitudes from two perspectives. The distance z is set to the same as used in the experiments. The Z axis (not labeled) shows the relative amplitudes A/A_0.

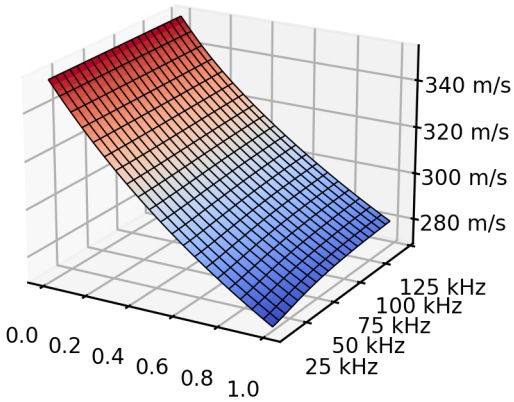

Figure 2.6: The simulated speed of sound in a surface with frequency and CO_2 concentration.

2.7 Machine Learning

In this work machine learning will be used to create predictive models for gas composition sensing.

The purpose of utilizing machine learning is to be able to create robust estimators which does not necessarily require knowledge of the complex nature for each specified gas.

2.7.1 Regression

Linear regression is a simple but fundamental form of regression, and is described as:

$$X\beta = \hat{y} \tag{2.7.1}$$

where X is a matrix of dependent variables (features), β is the vector of regression coefficients and $\hat{y}$ is the predicted independent variable (predicted target).

In eq. (2.7.1) the output has a single dimension, but if the coefficients was a matrix with N columns the model gives an N-dimensional output.

Linear Least Squares

The linear least squares problem is to find the coefficients, β, that minimizes $||X\beta - y||_2^2$, where y is the target. This is often done using singular value decomposition [21].

The function to minimize, $||X\beta - y||_2^2$, is called the objective function.

Regularization

Most algorithms need some sort of regularization to avoid overfitting. Overfitting occurs when the machine learning model tries to explain unlogical variations in the training set. This often caused by noise or overly complex modeling which is not present in the validation set. The validation set is used to verify that the model is performing well: the model is overfitted if the training accuracy is notable larger than the validation accuracy.

L1 and L2 regularization are techniques where the target is to minimize the complexity of the weight coefficients (β). This helps reduce the complexity of the machine learning model. Using L2 regularization the following term is added to the objective function [21]:

$$\alpha \cdot ||\beta||_2^2 \tag{2.7.2}$$

where α is the regularization strength. For L1 regularization the root and power is set to 1 ($||\beta||_1^1$). This means that the L1 regularization does not penalize fluctuations in the coefficients as much as the L2 regularizer does.

Many other regularization techniques exist where many are made for specific algorithms, for example the kernel parameter, γ, for the Support Vector Machine (SVM).

Support Vector Machine

The SVM is a popular algorithm in many fields. It has especially shown its strength in various medical applications like tumor detection [22].

Its main application is for classification tasks since it is creating a hyperplane for separation of classes, but the libsvm implementation uses the same techniques for regression which has been proved to be a good regressor [23].

The machine uses a kernel function with a set of support vectors for calculating the output variable. The gaussian Radial Basis Function (RBF) is the most common kernel and is calculated as:

$$K(x_i, x_j) = e^{-\gamma||x_i - x_j||^2} \tag{2.7.3}$$

where γ is a regularization parameter for the kernel.

2.7.2 Neural Networks

Neural networks have existed for many decades but has recently experienced an increase in usage as it has shown its strength in many fields like image analysis [24].

The neural network is composed of a set of layers each having a function $f_i(X_i)$ such that the network can be represented as $f(X) = f^N(\dots f^2(f^1(X)))$, where N is the number of layers. Each layer consists of parallel estimations known as units. These resemble the neurons in the human brain where the name "neural network" comes from.

A Convolutional Neural Network (CNN) is a network which uses convolutions to extract information from the data. This is very useful where information is dependent on the position of the variable in, for example, a grid. Normally, the first layers of a convolutional network uses convolutions, then information is gradually extracted using normal dense (feed forward) layers.

CNN's are widely used in image classification, but can also be applied to time series or similar data. The ultrasonic signals are time series. Therefore, a CNN can give useful results in this work.

2.7.3 Preprocessing and Training Techniques

Raw unprocessed data is seldom used to train machine learning models on. Prior to deploying the algorithm the data often needs to be transformed into a representable state.

This is especially true for the received ultrasonic signals, these are oscillating signals where the time for the discrete samples is not necessarily consistent. The methods used for transformation are presented in section 4.3.

Standardization

When standardizing a training set all features are set to have a standard variation of 1 and values centered around zero:

$$x_i' = \frac{x_i - \mu}{\sigma} \tag{2.7.4}$$

where x_i is the ith training feature vector, x_i' is the standardized vector, μ is the mean of x_i and σ is the standard deviation of x_i.

This is useful to make values comparable that otherwise would have completely different scales, which is important due to regularization of weights.

2.7.4 Evaluation

A machine learning model can be evaluated with many methods which might give different results when it comes to model selection.

The Mean Absolute Error (MAE) is a very intuitive evaluation metric for error estimation. It is calculated as the mean of the absolute residuals:

$$MAE = \frac{1}{N}\sum_{i}^{N} |r_i| \tag{2.7.5}$$

where N is the number of samples and r is the residuals.

The residuals are calculated as the distance from the actual value to the predicted value:

$$r_i = y_i - \hat{y}_i \tag{2.7.6}$$

where y is the vector of actual values, $\hat{y}$ is the vector of the predicted values.

Mean Squared Error (MSE) is better at penalizing errors, but can give unreliable results if there are many outliers:

$$MSE = \frac{1}{N}\sum_{i}^{N} r_i^2 \tag{2.7.7}$$

Root Mean Squared Error (RMSE), the root of MSE gives a more intuitive metric which has the same magnitude as MAE:

$$RMSE = \sqrt{\frac{1}{N}\sum_{i}^{N} r_i^2} \tag{2.7.8}$$

The coefficient of determination, R^2, is a metric describing the linear relationship between two variables. In linear regression it is a usable metric to describe how good fit the model actually has. R^2 is calculated as:

$$R^2 = 1 - \frac{\sum_i r_i^2}{\sum_i [y_i - \mu_y]} \tag{2.7.9}$$

where μ_y is the mean of the target, ie sum of squared residuals divided by the sum of squares.

If the R^2 is 1 the model has a perfect fit, a value of 0 indicates that the model is as good as a model giving the expected value of y (μ_y). A negative value indicates an even worse fit and should not be considered for predictions.

3. Review of Related Work

In this chapter the objective is to review existing work on applying acoustics as a method of recognizing different gas mixtures.

3.1 Ultrasonic Sensing

There seems to be little ultrasonic sensing technology used in production. However, recent research on acoustic molecular relaxation has revealed some proposed methods using ultrasonic transducers for gas sensing.

3.1.1 Attenuation Based Detection

These sensors can be used for binary classification or anomaly detection.

In [25] the authors used a coupled transducer pair on a direct gas flow of air. When switching to pure nitrogen they showed that an increase in attenuation gives a shift in the sensor output which can be measured within few milliseconds. The proposed use case is real-time gas monitoring, where the system can detect changes in the concentration, but the application is not able to identify the actual mixture.

3.2 Sensing Based on Relaxation Models

Even tough acoustic relaxation has been known for many decades [14], recent studies of multimode relaxation processes has increased the interest of reconstructing the relaxation processes from ultrasonic measurements.

The Quantitative Acoustic Relaxation Spectroscopy is a method proposed by Petculescu and Lueptow in 2012 for moderate real-time monitoring of gas compositions. Use cases mentioned are identification of contamination in air for mining safety and impurity detection in natural gases [16].

3.2.1 Reconstruction Algorithms

An accurate algorithm which reconstructs the relaxation processes in excitable gases is a challenging subject since most transducers have fixed frequencies.

In 2005 Petculescu and Lueptow proposed an algorithm requiring a two frequency measurement for capturing the primary relaxation processes in a gas mixture [13]. The algorithm can reconstruct the peak of $\alpha\lambda$ with a relative error of 15% and the relaxation frequency, f_{relax}, with a relative error of 11% in a mixture of 95%N_2 and 5%CO_2. This model was used for creating a prototype acoustic gas sensor in [26].

A real-time monitoring application was proposed in [27] by Hu, Wang, Zhu, Zhang, Liu, and Xu. Using the peak of a reconstructed relaxation spectrum, a

method for monitoring the actual concentration is proposed. The method is based on the two frequency reconstruction mentioned in [28] which is used to capture the primary relaxation frequency. This algorithm can however only capture a single relaxation process.

In [18] an algorithm which captures the entire relaxation spectra for a gas composition is proposed. Using frequency measurements which cover the interior relaxation processes the entire spectra is reconstructed based on the theories in [15]. The same model is applied for reference in this work.

3.2.2 Classification of Mixtures Based on GARAS

Jia, Yu, Du, and Wang used wavelet decomposition on synthesized relaxation spectra for mixture classification in [29]. Using wavelet Multi Resolution Analysis (MRA) and feature extraction a SVM was trained on the relaxation spectrum (see section 2.5.2).

The problem was solved as a classification problem for mixtures obtained from the theoretical model for a total of four mixtures. Even tough the value of training a machine learning application on a theoretical model is questionable, the model also gives full testing accuracy. This shows that the relaxation spectrum is distinguishable under the right conditions. The same methods can be used for a more general approach where the gas composition is solved as a regression problem.

Another problem is that this requires a fully reconstructed relaxation spectrum. This requires many frequency measurements as seen in [18].

3.2.3 Detecting Inflection Point of Frequency-dependent Velocity

In [17] the authors of the relaxation models used speed of sound measurements for estimation of gas composition.

Using a reconstruction algorithm the authors managed to locate the inflection point of the frequency dependent speed of sound curve (see the real part of fig. 2.4). The inflection point is located at the frequency which corresponds to the primary relaxation mode in the mixture. Using the location of the inflection point the final composition of a CO_2-N_2 mixture was calculated with high accuracy.

The method is highly relevant but lacks justification of measurements in mixtures where the speed of sound contribution of relaxation is indistinguishable from noise like CO_2-N_2 with high concentration of nitrogen. Looking at fig. 2.6 it is evident that the sound speeds do not decrease enough for mixtures with a carbon dioxide concentration below $\approx 30\%$.

3.2.4 Concentration Measurements from Mixtures of CO_2 and N_2

In [30] the authors used experimental results from a good spectrum of the CO_2-N_2 spectra similar to what is done in this work.

Using a two frequency measurement, the concentration is estimated based on the reconstructions from the decompositions in [28]. A fitting method is used to establish the relationship with the actual sound absorption from relaxation, $\mu(\omega)$. Using these values the concentrations are measured with errors ranging from 2% to 10% absolute molar concentration.

This work is the most relevant to the methods applied here since it uses a set of nitrogen and carbon dioxide mixtures for concentration prediction.

4. Method

Based on the theories for attenuation of ultrasonic waves it becomes obvious that sound waves can be used to model a gas-composition detection algorithm utilising ultrasonic transducers.

Thanks to relaxation effects there are differences in the attenuation at different frequencies. This makes it possible to distinguish mixtures that otherwise would have equal attenuation, provided that there are significant relaxation effects. This could be done using the theoretical models, as pointed out in [16, 17], which requires accurate data about relaxation modes and the physical properties of the gas mixture. Using machine-learning techniques the need for physical data is effectively exchanged with experimental data.

This chapter provides several methods for gas composition sensing using machine learning and known theories based on experimental data achieved using off-the-shelf transducers in a custom-made rig.

Figure 4.1 shows the relationship between the theoretical and predictive model. Using machine learning on experimental raw signals the predictive model does not need to be dependent on the physical properties.

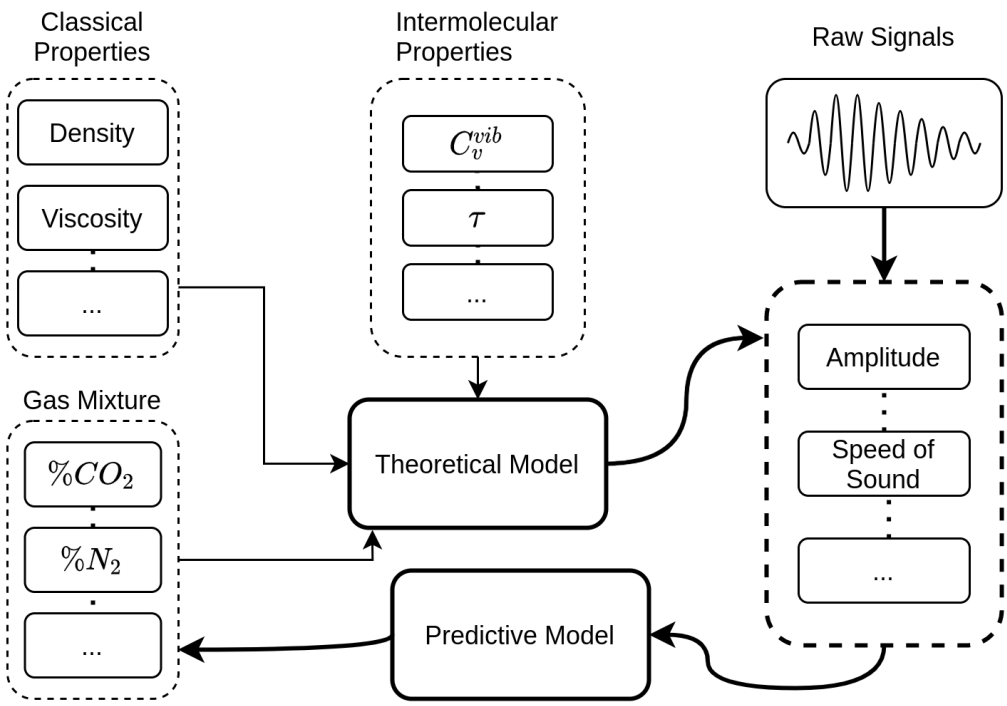

Figure 4.1: Model diagram showing the relationship of the theoretical model and the gas-sensing models.

4.1 Experimental Test Rig

Data is acquired using a test rig that was constructed for the purpose of transmitting and receiving ultrasonic signals in calibrated gas mixtures.

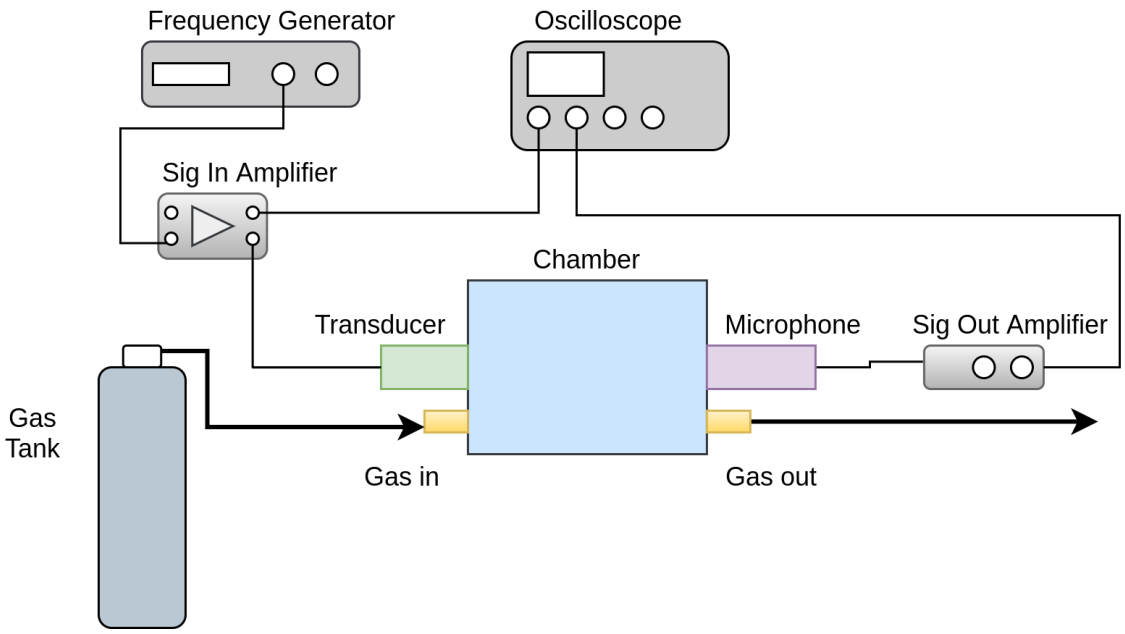

Figure 4.2: Chart showing the setup of the rig.

4.1.1 Equipment

The following is a list of the main equipment used for the experiments:

- Brüel & Kjær Ultrasonic Microphone
- Brüel & Kjær Pre-Amplifier (Sig Out)
- Chamber
- Oscilloscope
- Frequency Generator
- Amplifier (Sig In)
- Transducers
- Gases (mixtures of nitrogen and carbon dioxide, see table 4.3)

4.1.2 Chamber

The chamber holds the gas during the measurements. It is not designed for pressurization and should hold atmospheric pressure.

Since echoes from the structure around the gas might be a problem the inner of the chamber is covered with a sound-absorbing material.

The endcaps have fittings on each end which is used for mounting the transducer and microphone. The transducer fittings are made to simplify the change of transducer. In addition, the end with the microphone has a gas outlet valve, and the end with the transducer has two gas inlets.

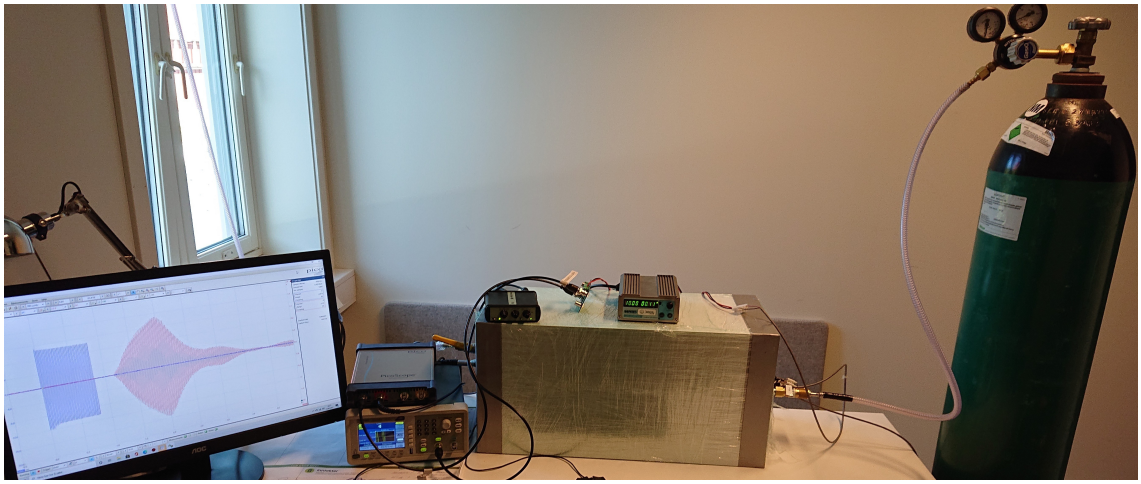

Figure 4.3: Picture of the test rig during operation.

4.1.3 Transducers

In table 4.1 below all transducers used for the experiments are listed.

Table 4.1: List of transducers and relevant parameters

Id	Drive frequency /kHz	Max input voltage / V_{pp}
$Tx1$	25.0 ± 1	56
$Tx2$	32.8 ± 1	56
$Tx3$	40.0 ± 1	56
$Tx4$	49.5	
$Tx5$	60.0	
$Tx6$	50.0	1000
$Tx7$	100 ± 8	600

Signal in

The signal in is generated in the frequency generator. It is set to send bursts of a specific number of cycles. The signal is amplified in the Sig-In amplifier which gives a signal amplitude of approximately ±12V ($V_{pp} \approx 24$V). Some transducers can handle higher voltages (up to 1000 V_{pp} for tx6). For these transducers the signal is additionally amplified using a transformer with a ratio of 1:6 which is attached after the amplifier.

Signal Out

A high-frequent microphone is used to sample the signals on the receiver side. The Sig-Out amplifier has settings of 1x, 10x and 100x. For the transducers giving low impulses it is set to 100x, and 10x for the remaining transducers (see table 4.4).

The signal is then captured in a PicoScope™ oscilloscope.

4.1.4 Characterization of Transducers

In order to establish a baseline of how the transducers will behave and for verification of the resonance frequencies, a characterization of the transducers is useful.

The transducers can be characterized using the equivalent RLC || C circuit in fig. 4.4 [31].

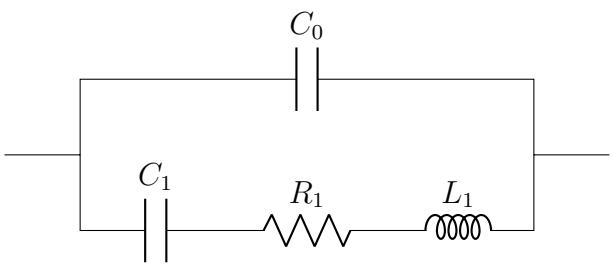

Figure 4.4: Equivalent circuit for piezo-electrical transducers

The resonance frequency can be calculated from the RLC arm of fig. 4.4. Resonance occurs when the resistance is at its minimum when $X_C = X_L$:

$$\begin{aligned} X_C = X_L &= \frac{1}{\omega_r C_1} = \omega_r L \\ \implies \omega_r &= \frac{1}{\sqrt{L_1 C_1}} \\ f_r &= \frac{1}{2\pi\sqrt{L_1 C_1}} \end{aligned} \tag{4.1.1}$$

Using an impedance analyzer the equivalent values C_0, C_1, R_1, L_1 have been found in table 4.2. The resonance frequency f_r is calculated from eq. (4.1.1).

Table 4.2: Transducer characteristics

Id	f_r/kHz	C_0/pF	C_1/pF	R_1/Ω	L_1/mH
$Tx1$	25.6	2498	293.5	671.7	131.9
$Tx2$	33.0	2301	125.0	462.7	186.2
$Tx3$	39.1	2617	144.0	764.8	114.8
$Tx4$	50.1	495	20.2	1920.8	500.4
$Tx5$	60.3	778	123.3	211.3	56.5
$Tx6$	55.2	1059	353.8	154.0	23.5
$Tx7$	98.0	633	119.8	511.2	22.0

4.2 Data Acquisition

The transducers from section 4.1.3 and the test rig is used to obtain data for a set of N_2 —CO_2 mixtures.

4.2.1 Gas Compositions

In table 4.3 the gas mixtures for the experiments are listed. The fraction (X_n) indicates the molar fractions. These are all calibrated mixtures of the Mapcon® series from Nippon Gases®.

Table 4.3: Gas compositions for the experiments

Id	X_{CO2}	X_{N2}
$n2$	0.0	1.0
$nd20$	0.2	0.8
$nd30$	0.3	0.7
$nd50$	0.5	0.5
$nd60$	0.6	0.4
$co2$	1.0	0.0

4.2.2 Estimation of Experimental Parameters

Since the transducers have different characteristics the transmitted burst is modified to yield good results. These parameters are estimated when the gas-chamber is filled with pure nitrogen.

The peak-to-peak voltage (V_{pp}) is set as large as possible to give high impulse responses on the microphone. Either max V_{pp} from table 4.2 or the maximum of the test-rig ($96V_{pp}$) is used. The voltage is $96V_{pp}$ on the transducer when the generator is set to 1000mV and the transformer is used.

The number of pulses of the transmitted burst is set to maximize amplitude of the received signal. When echoes are observed the number of pulses is reduced such that the pulses do cause interference.

The frequency of the transmitted burst will vary. It was observed that the optimal frequency changes over time, this is possible due to some transducers requiring to "warm up", for these transducers the optimal frequency are estimated after being driven for some time (typical 15 minutes). The frequency is set such that the received response has high amplitude which should be at the resonance frequency. However, it can be observed that the frequency differs from table 4.2. This might be caused by the warm-up period or errors from the impedance measurement. For the analysis and experiments the frequencies found here (in table 4.2) will be used instead.

Table 4.4: Experimental parameters

Id	V_{ppg}/mV	N_{cyc}	Frequency/kHz	Transformer	Pre-amp
Tx_1	350	33	25.0	Yes	100x
Tx_2	350	33	32.9	Yes	100x
Tx_3	350	20	40.0	Yes	10x
Tx_4	1000	16	49.7	Yes	100x
Tx_5	800	12	59.7	No	100x
Tx_6	800	9	49.9	Yes	100x
Tx_7	800	7	102.5	Yes	100x

The voltage V_{ppg} in table 4.4 is the voltage of the generator setting.

4.2.3 Acquiring Signals

The general procedure is described in appendix A.

All gas mixtures in table 4.3 are tested with each of the transducers from table 4.1. For each combination of transducer and gas mixture a set of minimum three runs are done. The PicoScope software for the oscilloscope stores 32 samples for each run.

4.3 Preprocessing

This section contains the methods used for preprocessing and extracting data from the ultrasonic signals, which will be used later for predictive models and comparison with the theoretical models.

4.3.1 Filtering of Signals

Signal filtering is used to remove unwanted noise and/or parts of a signal in order to isolate the interesting frequencies.

For measuring the burst response from the transducers, only the given resonance frequency is of interest. Other responses come from environmental noise and can typically be observed as high-frequency responses.

Applying a filter G in the frequency domain can be described as [32]:

$$X' = GX \tag{4.3.1}$$

X', X is the unfiltered and the filtered signal, respectively.

Forward-backward Filtering

Applying a Infinite Impulse Response (IIR) filter to a signal will almost always cause a phase delay. This is caused by the phase differences of the signal and the filter itself [32].

Changing the phase of the signal cause inaccuracy in the velocity calculation and should therefore be avoided. A method to avoid any phase shifts caused by filtering is to apply the filter twice, where the signal is time-reversed on the second filtering [33].

Any phase delay δ will then be reversed:

$$\begin{aligned} X''^R &= GX'^R \\ &= GG^R X^R \\ X'' &= (GG^R X^R)^R \\ &= GG^R X \end{aligned}$$

X'' is the forward-backward filtered signal. As a result, any phase delay will be zeroed out.

Forward and backward filtering does not give the same result as normal filtering, Gustafsson's [33] method for determining initial states will be used to avoid changes at the beginning and end of the filtered signal.

Figure 4.5 shows the received signal together with the filtered and the double-filtered signal. The signal was generated using Tx4 with the parameters in table 4.4 and the nd30 mixture (30%CO_2). Filtering is done using a Butterworth IIR filter having bandpass cutoffs at 30kHz and 60kHz. Looking closely it can be observed

that the phase has changed after the initial filtering, but is normalized after the reverse filter.

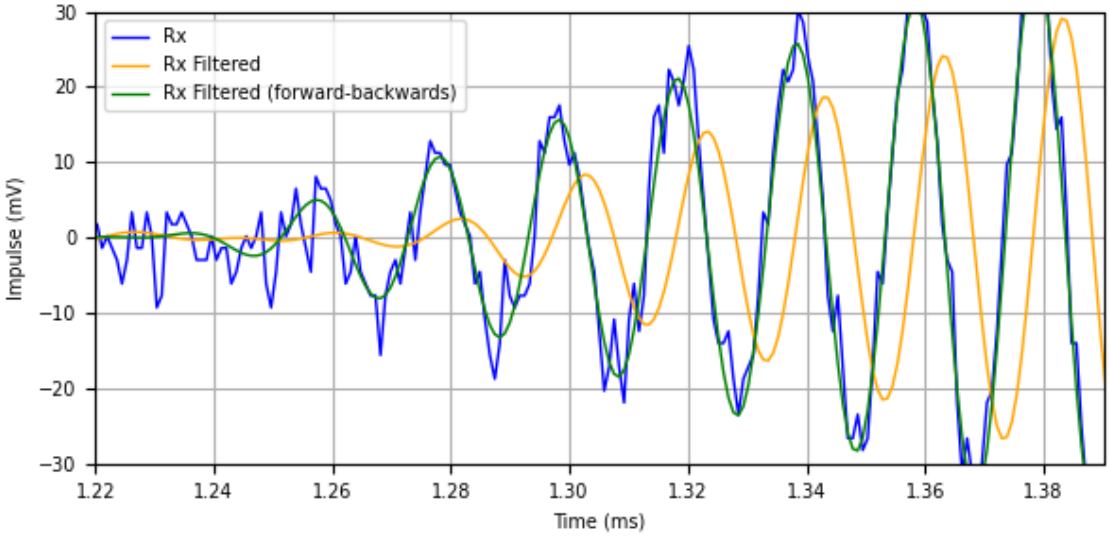

Figure 4.5: Comparison of raw and filtered signal with forward-reverse filtering

All signals are preprocessed with a bandpass filter having cutoffs at ±20kHz around the transducer's resonance frequency. As seen in fig. 4.6 the filtering enchants the signal largely and can find responses that are barely visible prior to filtering.

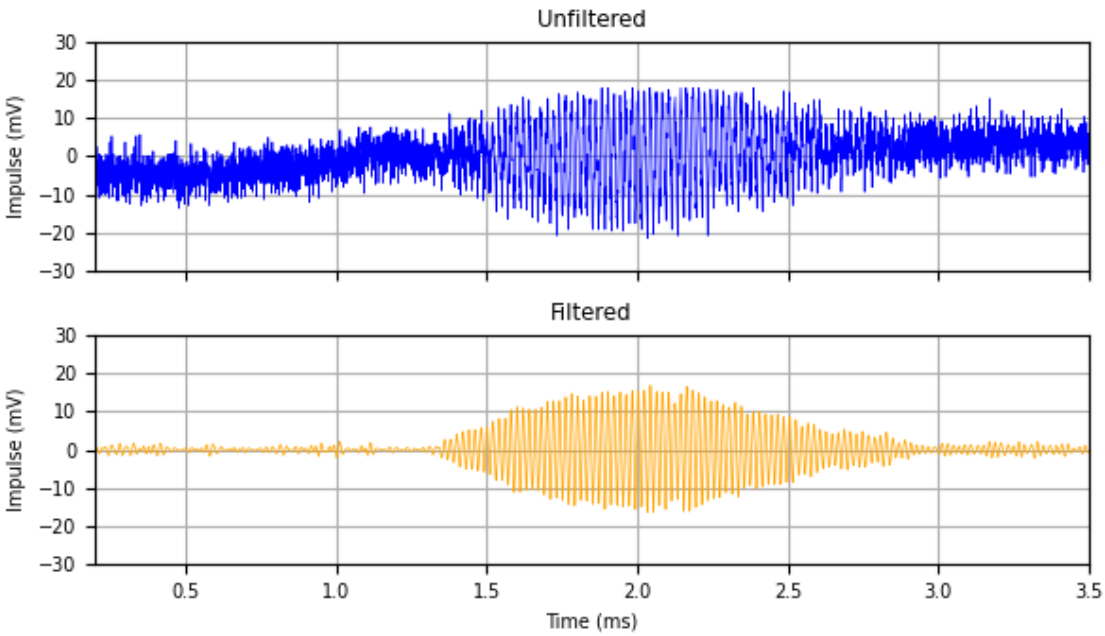

Figure 4.6: Comparison of unfiltered and filtered signal (Tx4)

4.3.2 Calculating Attenuation of Signals

The amplitude can be obtained from the signal as the maximum of the absolute signal:

$$A = \max_t |x(t)| \tag{4.3.2}$$

The initial amplitude A_0 depends on the transducer, applied voltage, frequency and number of waves. For any given transducer A_0^i is constant for all measurements.

In [26, 30] the amplitudes were corrected for diffraction. This is not needed using the method described here since it is implicit in the calculated initial amplitude, A_0, and is constant for the given frequency.

A_0, can be obtained for transducer i from eq. (2.4.1) as:

$$A_0^i = \frac{A_x^i}{e^{-z\alpha_{xi}}}, \quad \alpha_{xi} = \alpha_c(\omega_i) + \alpha_r(\omega_i) \tag{4.3.3}$$

where i is the transducer id, $\omega_i = 2\pi f_i$ is the angular frequency applied to the transducer and x is the gas composition from table 4.3. However, this requires that the predictions $e^{-z\alpha_{xi}}$ are correctly explaining the attenuation of the received signal which might be prone to errors.

The relative amplitude A/A_0 is given as:

$$\frac{A}{A_0} = e^{-z\alpha} \tag{4.3.4}$$

It is beneficial to use the relative amplitude as it is normalized and gives equal scale for all transducers. A_0 is found using a calibrated gas from table 4.3. For this, nitrogen was chosen since it primarily is not affected by relaxation and should therefore give more confident results with little noise. For each training sample, A_0^i is calculated, and then the average is taken as the initial amplitude.

Table 4.5: Initial amplitudes for the transducers

Id	Standard Deviation	Coefficient of Variation	Mean	Outliers
$Tx1$	35.58	0.0030	11714.81	0
$Tx2$	8.08	0.0013	6175.13	2
$Tx3$	14.41	0.0102	1409.88	0
$Tx4$	1.35	0.0041	328.48	0
$Tx5$	13.31	0.0075	1784.44	0
$Tx6$	27.99	0.0037	7643.96	0
$Tx7$	136.86	0.0094	14618.12	0

In table 4.5 the average of the initial amplitudes are calculated using eq. (4.3.4). The Coefficient of Variation is the relative standard deviation ($CV = \sigma/\mu$, where σ, μ is the standard deviation and mean respectively). It shows that the highest variation is at Tx7 and Tx3, 0.01 is still reasonable low. The outliers are calculated as values outside the Interquartile Range (IQR) multiplied with 1.5.

In fig. 4.7 the data from table 4.5 is represented using box-plots.

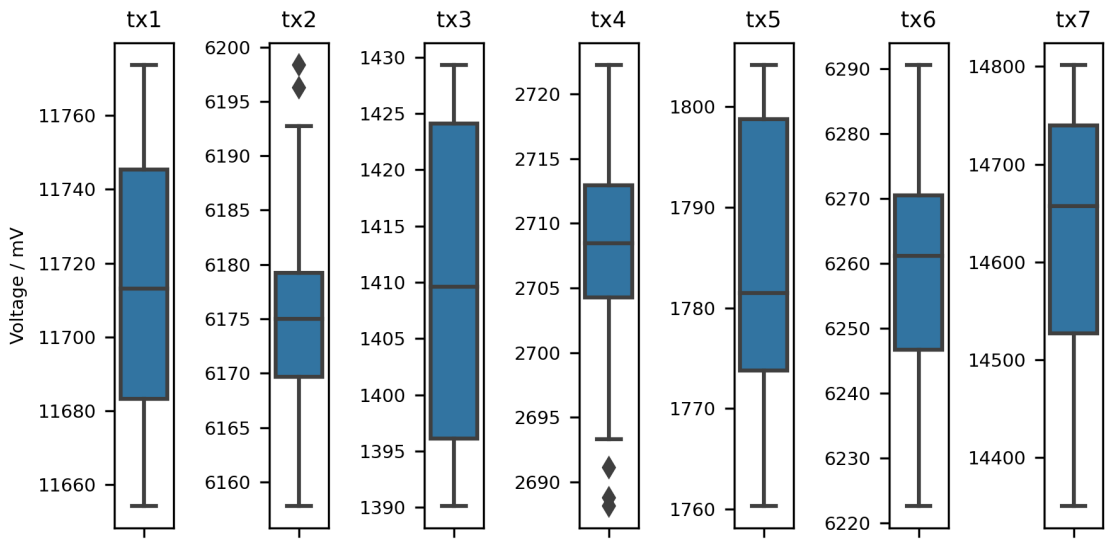

Figure 4.7: Boxplot of the calculated initial amplitudes for the transducers from table 4.2. Outliers are marked as diamonds, the whiskers (horizontal lines) show the outlier limits of 1.5 times the IQR, and the box shows the quartiles.

4.3.3 Noise Detection

Looking at fig. C.4 it can be seen that for larger concentrations of carbon dioxide the speed measurements can give incorrect results and this increases when the signal is lost in noise. This causes the speed of sound measurements to be more or less random in the situations where the signal disappears. Most machine learning algorithms have little or no error correction and cannot identify a feature as "noisy" in specific circumstances. The normal result when training models on such features is heavy regularization on the relevant model weights which cause the features, which are otherwise useful if correct, being ignored by the model.

This can be corrected by adding noise-detection for reducing the speed of sound measurements in noisy measurements. The idea is to apply a multiplier to the speed of sound measurements which degrades heavily when the Signal to Noise Ratio (SNR) decreases to a certain level.

When detecting noise SNR is an often used measurement technique for explaining the relationship between the signal and the noise. There are multiple methods for calculating SNR [34, 35]. Most important is that it gives a relationship between the signal and noise where a SNR of 1 or lower indicates that the noise and signal is indistinguishable.

In this work the ratio will be defined as follows:

$$SNR = \frac{\mu_{|s|}}{\sigma_n} \tag{4.3.5}$$

where $\mu_{|s|}$ is the mean of the absolute values in a selected portion of the signal, and σ_n is the standard deviation of the sample prior to the signal wavelet.

Since the signals cannot be received earlier than 1ms after transmission the deviation in noise is calculated in the period from 0 to 1ms. The absolute mean of the signal is calculated in the period from 1.25 to 1.75ms, which should include all signals as can be seen in appendix C.

As seen in fig. 4.8 the requirements for the ratio fits well with eq. (4.3.5). The value falls below 1 only in samples without signal (tx7 in CO_2), meaning that the definition of SNR is highly applicable in this case.

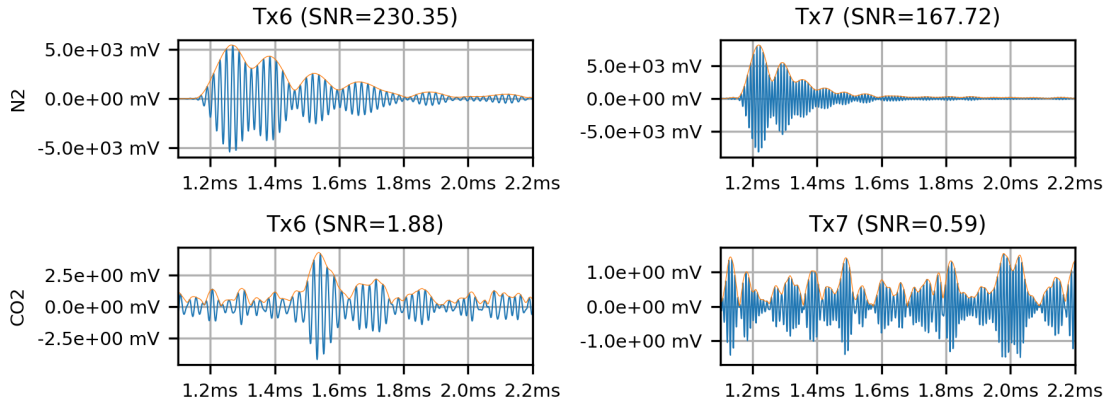

Figure 4.8: SNR in some samples from tx6 and tx7. The orange line is the envelope, and the SNR is shown in the subtitles. The plots in the right column are from tx7 which loses signal in the nd50 mixtures and above. The plots in the left column are from tx6 which has signal in co2. The upper row consists of samples in nitrogen and the lower row are from carbon dioxide.

The decay function $\epsilon(x)$ will then be defined as a sigmoid:

$$\epsilon(x) = \frac{1}{1 + e^{-\alpha(SNR(x)-\beta)}} \tag{4.3.6}$$

where α is the decay strength and β is the center of the sigmoid. When $SNR(x) = \beta$ the decay is 0.5. The values for α and β were chosen in an iterative approach to make the speed of sound measurements from tx6 in co2 to be conserved and at the same time to decrease the calculations in tx7 for concentrations above 0.4. The most optimal values were found visually as $\alpha = 50$ and $\beta = 1.25$. The decay with these values are plotted in fig. 4.9. Any value multiplied by the decay will converge towards zero if the signal is expected to disappear in noise.

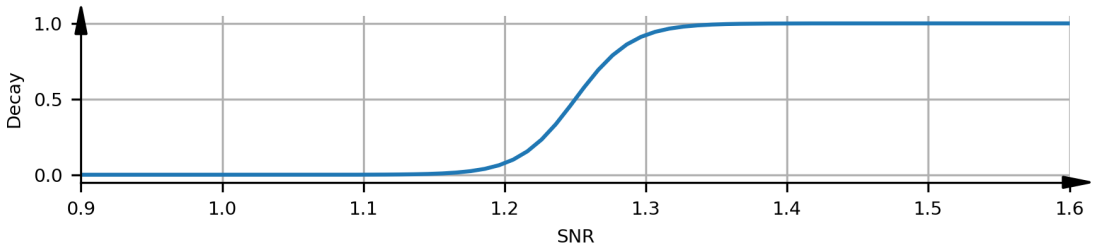

Figure 4.9: The decay as a function of SNR with $\alpha = 50$ and $\beta = 1.25$.

4.3.4 Transformation of Raw Signals

When looking at the raw signals it is important to consider that the signal strength varies by several orders of magnitude, as can be seen in appendix C. Since the machine learning algorithms normally does not scale inputs logarithmically this has to be done as a preprocessing step. The transformation takes the logarithm of the envelope of the signal, it is mathematically described as:

$$x' = log\left[|x + iH(x)| + \epsilon\right] \tag{4.3.7}$$

where x' is the transformed signal, $x + iH(x)$ is the analytic signal of x, $H(x)$ is the hilbert transformed signal [32], ϵ is a very small number to prevent taking the logarithm of zero.

The original raw signal is filtered and then eq. (4.3.7) is applied. Then the signal is linearly interpolated to a time-range from 1.0 ms to 2.2ms with 200 samples. In fig. 4.10 an example from the tx6 transducer is shown. Note that after transformation the values have approximately the same magnitude in nitrogen and carbon dioxide. This is not the case prior to transformation where the amplitude in nitrogen is approximately 2000 times larger than in carbon dioxide.

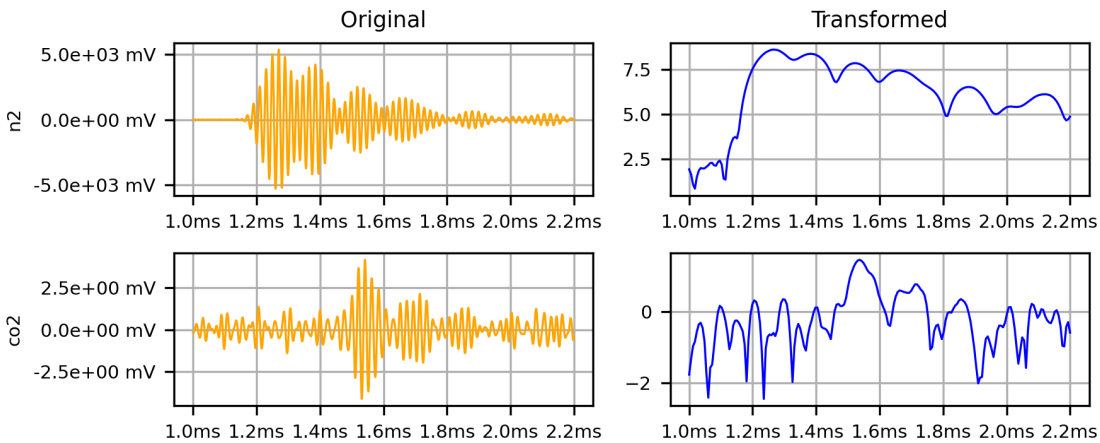

Figure 4.10: Transformation of raw signals for the predictive models. These samples are from tx6 in nitrogen and carbon dioxide. The plots on the left side are the original filtered signals, and the plots on the right side the transformed signals.

The number of samples in the transformed signal was estimated experimentally, which lead to a total of 200 samples being chosen. This gave good results for all models using this transformation.

4.4 Estimation of Speed of Sound

The speed of sound is an important parameter for composition detection and should be calculated as precisely as possible. It is also a part of the verification of the relaxation and mixing models.

By knowing the distance between the microphone and the transducer the speed is achieved using the definition of velocity:

$$c = \frac{z}{\Delta t} \tag{4.4.1}$$

where z is travelled distance, Δt is the calculated time-delay, c is the speed of sound. Since the distance z is known, Time Delay Estimation (TDE) will be used to estimate Δt.

The transmission from the frequency generator to the microphone can be described as a Linear Time Invariant (LTI) system [36]:

$$x_r = x_g * h \tag{4.4.2}$$

where $*$ is the convolutional operator, x_r is the signal received on the microphone, x_g is the generated signal, and h is the system impulse response.

The impulse response can be decomposed to the relevant steps:

$$h = \tau * \eta * h_t \tag{4.4.3}$$

where η is noise, h_t is the impulse response of the transducer and τ is the impulse response of the time delay.

Since the impulse response of the transducer should be constant, the transmitted signal x_g is constant for all signals from the respective transducer independent of the gas mixture.

The transmitted signal x_g and the impulse response h_t is unknown. Instead of calculating time delay from the transmitted signal, the time delay is calculated from a calibration signal received in nitrogen, x_c.

Speed of the sound in nitrogen is calculated using eq. (2.3.1) and the constant time-delay from the transmitted signal to the calibration signal is calculated using eq. (4.4.1).

The total time delay of the transfer is then represented as:

$$\tau = \tau_c * \tau_\delta \tag{4.4.4}$$

or

$$\Delta t = \Delta t_c + \Delta t_\delta \tag{4.4.5}$$

where Δt_c is the time delay from the calibration gas, Δt_δ is the time delay between x_c and x_r. There are multiple methods for evaluating the time difference between a delayed signal.

4.4.1 Cross Correlation

A Generalized Cross-Correlator (GCC) takes a cross-correlation of two equal signals, giving a symmetric signal that can be used for TDE.

This is a widely used method for time-delay estimation, and is often robust to noise since noise tends to cancel out itself when correlating [37].

For two real signals f, g, the cross-correlation $f * g$ is the same as a convolution of the time-reversed complex-conjugate $\overline{g(-t)}$, such that $f * g = f * \overline{g(-t)}$.

If the noise is ignored the received signal is a delayed version of the calibrated signal, such that $x_r = x_c * \tau_\delta$. Then the correlation becomes:

$$\begin{aligned} x_r \star x_c &= (x_c * \tau_\delta) \star x_c \\ &= (x_t * \tau_\delta) * x_c(-t) \end{aligned} \tag{4.4.6}$$

Since convolutions are commutative eq. (4.4.6) is rewritten as:

$$x_r = [x_c(-t) * x_c(t)] * \tau_\delta \tag{4.4.7}$$

The signal $x_c(-t) * x_t(t)$ has its maximum at $t = 0$, then the delay Δt can be retrieved as:

$$\begin{aligned} \underset{t}{\operatorname{argmax}} [x_r \star x_t] &= \underset{t}{\operatorname{argmax}} [x_c(-t) * x_c(t)] - \Delta t \\ &= \Delta t \end{aligned} \tag{4.4.8}$$

where the argmax operator takes the maximum of the function and returns the corresponding time. Now Δt can be used with eq. (4.4.1) to find the speed of sound.

Note that the discrete time array is centered around zero. The actual time delay is therefore calculated as:

$$\Delta t = \underset{k}{\operatorname{argmax}} \left[x_r(k) \star x_t(k) \right] - N_k \frac{1}{2} \tag{4.4.9}$$

where k is the sample number, N_k is the number of samples.

4.4.2 Peak to Peak

The method used by Zhang, Wang, and Zhu was to calculate the time difference between the peak of two signals [17]. This can be done using the maximum amplitude calculated from section 4.3.2 for the calibration signal and the received signal.

If the signal is a clean wavelet and the highest point of the impulse is conserved from the transmission this method is expected to perform nearly perfect.

The peak to peak method seemed to outperform the GCC. However, it was observed that the largest point of the signal could be offset with some cycles which would give incorrect calculations in noisy environments. This can be seen in fig. C.4 in the nd50 and nd60 mixtures. In order to improve the method the peak of the envelope was taken, giving slightly better results.

4.4.3 Threshold

A single thresholding approach could also be used between two known signals. Since the amplitudes vary, the signals should be scaled to $A/A_0 = 1$. The threshold should be large enough to overcome noise caused by low amplitudes, like the signals from tx4 (fig. C.4).

4.4.4 Evaluation

The discussed methods are tested against the theoretical model in order to find the TDE model best suited for estimations.

Since errors in the model or experiments might occur the method giving the lowest variance for each gas/transducer combination was assumed to be more correct as long the error from the theoretical model was in acceptable range.

All signals are discrete. This means that the calculated time delay is a multiple of the sample period which was interpolated to 4ms / 5000 samples, giving an uncertainty in time of ±0.8µs. This should give an uncertainty of less than 0.05% for speed measurements in nitrogen and lower in the other mixtures since the time-delay is longer.

Overall, using peak to peak on the envelope of the filtered signals gave the best results. The method is therefore used for all speed of sound calculations. The results of the speed calculations using this method is represented in section 5.2.2.

4.5 Predictive Models

The predictive models are modeled to do the inverse of the theoretical model. Instead of predicting expected attenuation and speed of sound the sensing models takes a raw signal and gives the predicted gas mixture. This is illustrated in fig. 4.11. The goal is to not being dependent on the theoretical model for predictions since it is difficult to find reasonable properties to a large variety of gases. The models represented here only relies on the theoretical model for calibration. For prediction, the model takes the raw signals, applies the appropriate transformations and predicts the gas mixture.

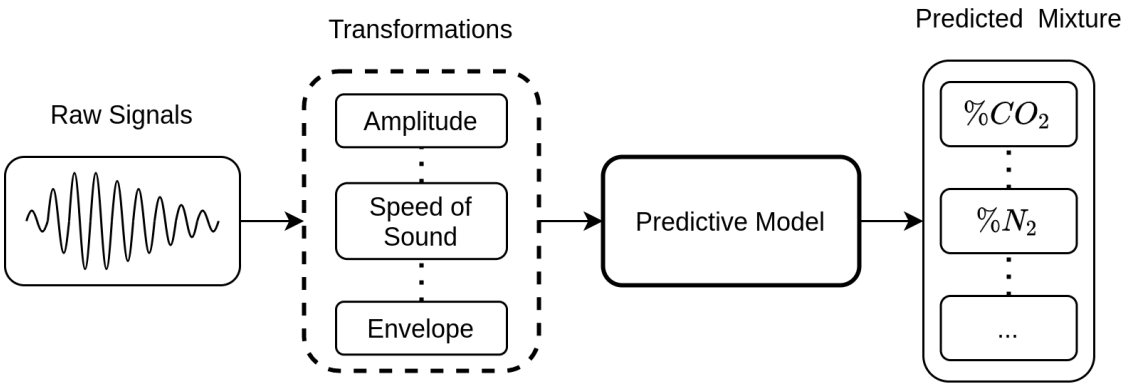

Figure 4.11: Diagram showing how the gas composition predictions are made.

4.5.1 Dataset Creation

The dataset is created by coupling each run-id with its file index for all transducers. Each measurement is represented once together with one measurement from each of the other transducers. The first run (run1) is kept for the test set.

Since the experiments only included specific gases a model might falsely look at the targets as classes instead of doing a reasonable regression which is a case of overfitting. This can be a problem for models which that normally prune to overfitting like random tree based models and neural networks. To identify models doing this the nd20 mixture (20%CO_2) is put in the testing set and is not used for training. If a model is overfitted, it can be seen that the predictions of nd20 are moved towards any of the other gas mixtures, affecting the validation metrics like MSE and R^2.

The test set now contains all the measurements in the first run (run1) and the experiments in nd20, giving a total of 268 test samples and 477 training samples. A complete overview can be found in table 4.6 below.

Table 4.6: Samples in the dataset

	n2	nd20	nd30	nd50	nd60	co2	Total
Test	32	108	32	32	32	32	268
Train	96	0	96	96	93	96	477
Total	128	108	128	128	125	128	475

4.5.2 Support Vector Machine Regression

This model uses a SVM with the amplitudes and decayed speed of sound in combination with the transformed raw signals from section 4.3.4 to do gas composition predictions.

The raw signals are transformed to 200 samples each in combination with the speed multiplied with the decay from section 4.3.3 and amplitude. Giving a total of $202 \cdot 3 = 606$ features (only three transducers were used due to the issues mentioned in section 5.1). Any other preprocessing steps like standardization did not improve the regression results and was therefore omitted.

The SVM has two hyper parameters, a regularization parameter C and a parameter for the RBF kernel γ. The optimal parameters in table 4.7 were found using cross validation on a parameter grid as recommended in the documentation of libsvm [23]. The best parameter combination was chosen from the model yielding lowest MSE.

Table 4.7: SVM - Optimal parameters

Kernel	C	γ
RBF (gaussian)	10^5	10^{-10}

Results

The support vector machine gave good results with an R^2 of 0.961997 for the test set, and 0.969982 for the training set. In fig. 4.12 the actual values are plotted against the predicted values.

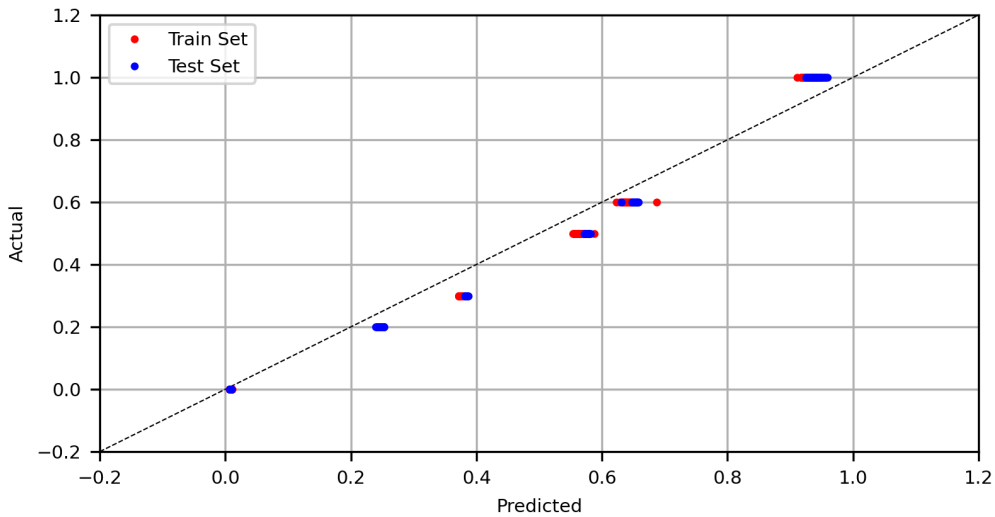

Figure 4.12: The results from the support vector regression, shows predicted fractions with actual fraction. The red dots are from the training set and the blue dots are from the test set.

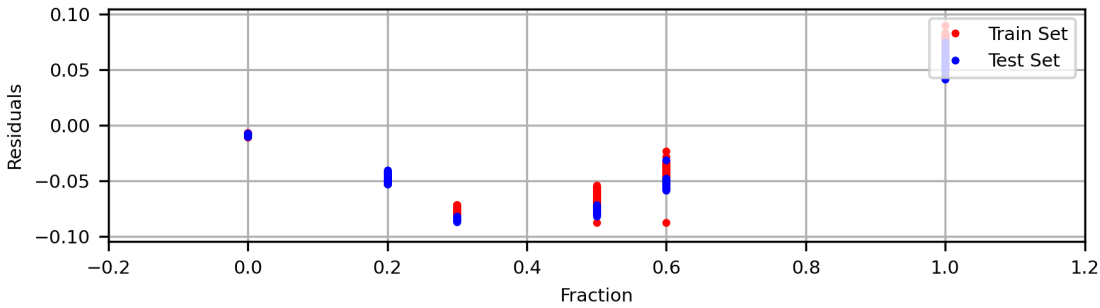

Figure 4.13: Residual plot from the support vector regression model, shows actual fractions against residuals. The red dots are from the training set and the blue dots are from the test set.

As seen in figs. 4.12 and 4.13 the SVM is not able to create hyperplanes which explains the data correctly. This can be seen as the predicted values have tight distributions which are offset from the correct values.

The output from the SVM can be calibrated using polynomial regression as interpolation. This is expected to improve the predictions significantly.

4.5.3 Calibration of the Support Vector Machine

As mentioned in section 4.5.2 the output from this model can take advantage of calibration. This means that a value is added to the output of the model. The value is determined based on the predicted value $\hat{y}$.

The linear regression with p polynomials will look like:

$$\epsilon = \begin{bmatrix} \hat{y}^0 & \hat{y}^1 & \hat{y}^2 & \dots & \hat{y}^p \end{bmatrix} \cdot \begin{bmatrix} c_0 \\ c_1 \\ c_2 \\ \vdots \\ c_p \end{bmatrix} \tag{4.5.1}$$

where $c_0 \dots c_p$ are the linear regression coefficients, $\hat{y}$ is the predicted fraction from the SVM and ϵ is the calibrated output. Then the calibrated $\hat{y}$ is recalculated as:

$$\hat{y_c} = \hat{y} + \epsilon \tag{4.5.2}$$

where $\hat{y_c}$ is the calibrated predicted value.

To give a good fit many polynomials are used with some L2 regularization. The calibration model ended with using 5 degrees of polynomials and a L2 regularization strength of $\alpha = 10^{-4}$.

As seen in fig. 4.14 below the calibration reduced the residuals significantly. The green dotted calibration curve in the upper shows the residuals from the calibrated fraction, such that the fraction is $\hat{y_c} = \hat{y} + \epsilon(\hat{y})$, and the residuals are $\epsilon(\hat{y})$. These are in the same plot for showing approximate good fit, but the curve is not valid outside the range of the dataset (0, 1). The calibration curve will be the origo for the new residuals $r_c = y - \hat{y_c}$ which can be seen in the lower plot where the new residuals are shown.

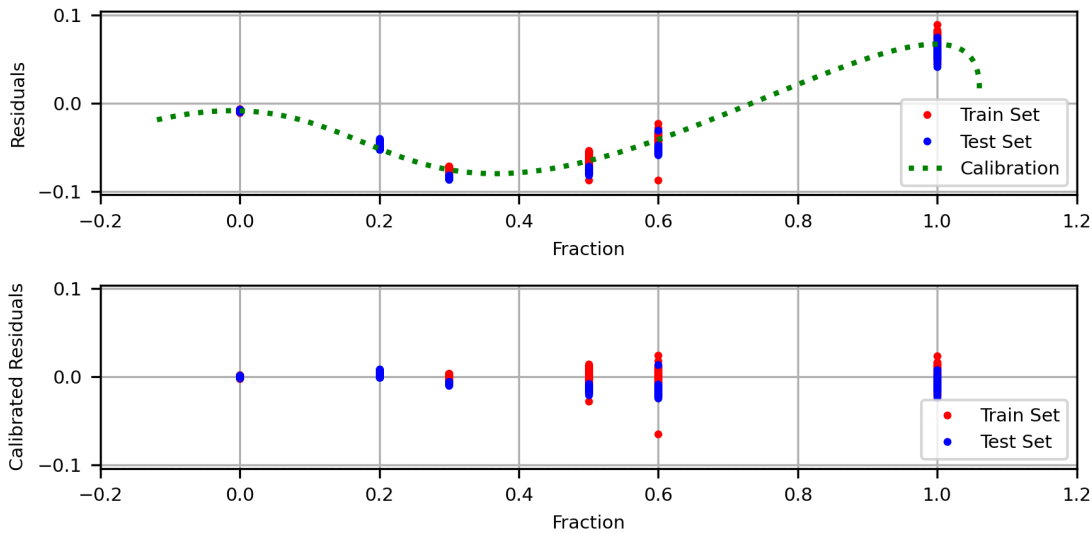

Figure 4.14: Residuals before and after calibration, the upper plot shows the original residuals with the calibration curve and the lower shows the calibrated new residuals.

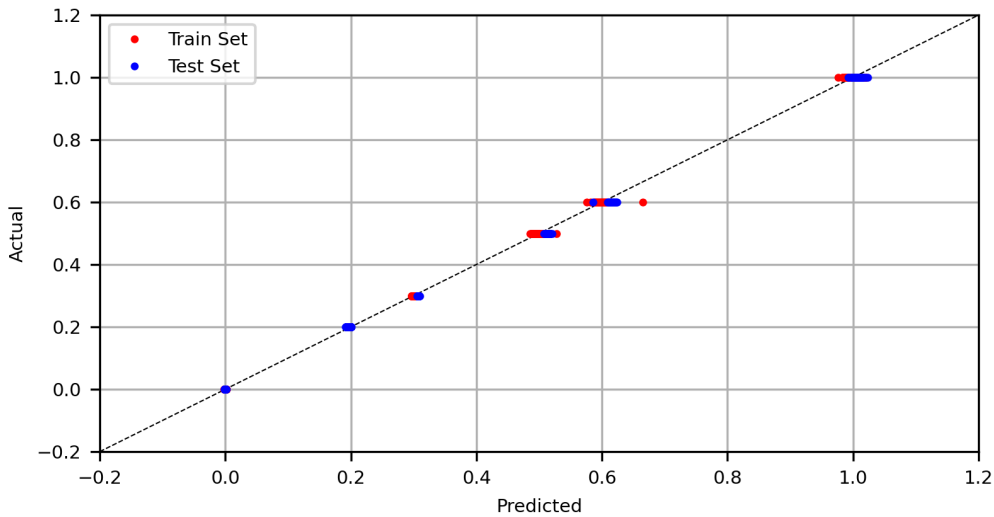

Figure 4.15: The new calibrated values plotted against the actual values for the SVM.

The calibration gave good results, with a new R^2 score of 0.999583 for the training set and 0.998997 for the test set. MAE for the training set is 0.004463 and 0.006969 for the test set.

4.5.4 Convolutional Neural Network

The previously models required the calibration curve from nitrogen due to the time delay and amplitude measurements. Using convolutions a model might look at the raw signal samples instead of extracting features like delay and amplitude. The neural network is only trained on the transformed signal from section 4.3.4.

Model Construction

The model is simple and constructed with few hidden layers. This is to prevent overfitting and reduce complexity. The nature of the problem is not expected to require complex architectures.

Table 4.8: Architecture of the convolutional neural network.

Type	Activation	Number of units
Convolution 1D	Tanh	32
Convolution 1D	Tanh	64
Dense	Tanh	16
Dense	Linear	1

The model was trained with a batch size of 32 random samples from the training set at 150 epochs. This means that the model has seen the training set 150 times and updated the weights accordingly. Weights were updated with the RMSProp (Root Mean Square Propagation) optimizer [38].

Results

In fig. 4.16 the actual values are plotted against the predicted values. Note that even though the model has never seen the nd20 mixture (at 0.2 co2) it still predicts this mixture accurately.

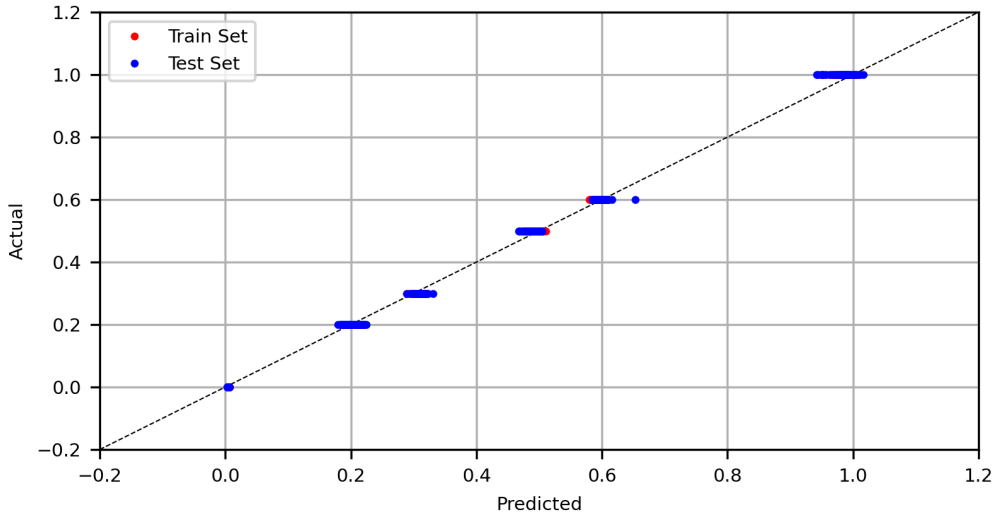

Figure 4.16: The results from the CNN, shows predicted fractions with actual fraction. The red dots are from the training set and the blue dots are from the test set.

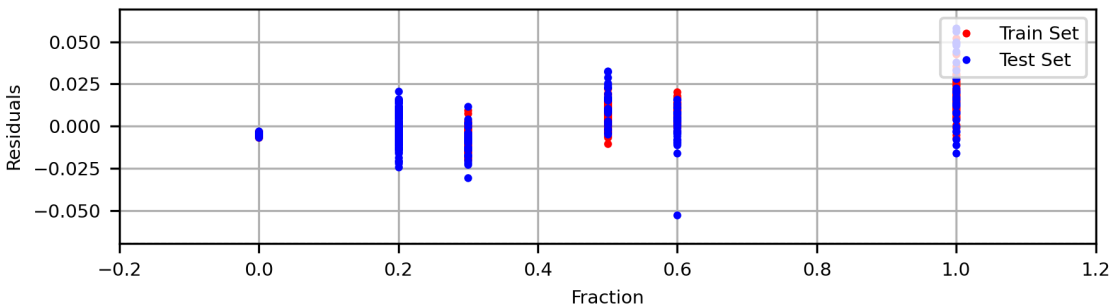

Figure 4.17: Residual plot from the CNN model, shows actual fractions against residuals. The red dots are from the training set and the blue dots are from the test set.

As seen in figs. 4.16 and 4.17, the model showed good results for both training and test sets. The MAE was estimated to 0.009145 for the test set, and coefficient of determination (R^2) was 0.997974.

5. Results and Discussion

5.1 Analysis of the Sample Signals

In appendix C sample signals for all transducers and gases are shown.

By roughly looking at the samples it can be concluded that there are unwanted effects in the received samples. The actual cause of the variations is unknown, but they seem to be constant for the relevant transducer.

One possible cause might be that the gas affects the transducers vibration and resonance. This can be seen in the low-frequency transducers tx1, tx2, and tx3 (figs. C.1 to C.3 in appendix C).

5.1.1 Echoes

Echoes from the surrounding materials are also present, in fig. 5.1 below it can be seen that there is a second pulse at 3.6ms in nitrogen. This is probably caused by reflections from the gas chamber.

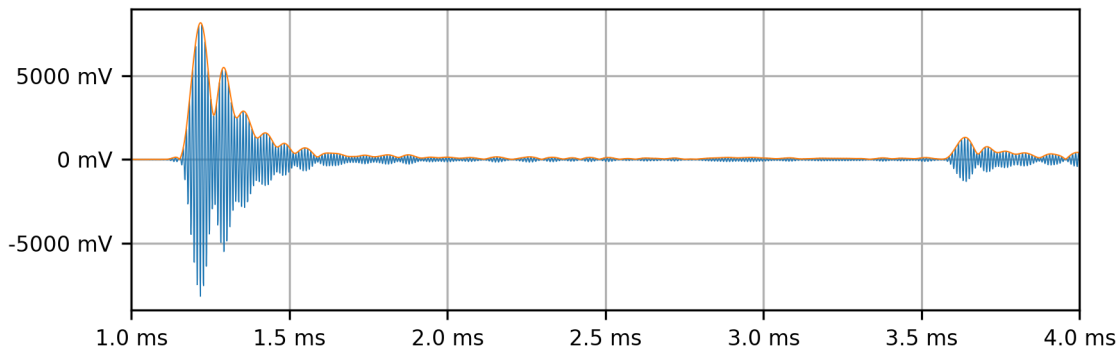

Figure 5.1: Echo in nitrogen (nd20) using Tx7 (100kHz). The orange line is the envelope calculated using hilbert-transforms.

In fig. 5.2 it can be seen that echoes disturb the major wavelet. There are at least 4 major reflections after the original wavelet. Since the speed of sound changes with higher concentrations of carbon dioxide the time delay between each echo is larger in the nd60 mixture. The number of cycles could not be set larger in nitrogen due to the second echo since it would have caused interference with the original wavelet. The interference would then have caused the amplitude and speed calculations to be incorrect for nitrogen and mixtures with low carbon-dioxide concentration. In mixtures with higher concentrations of carbon-dioxide this is not a problem due to the reduced speed of sound which causes the echo to arrive later.

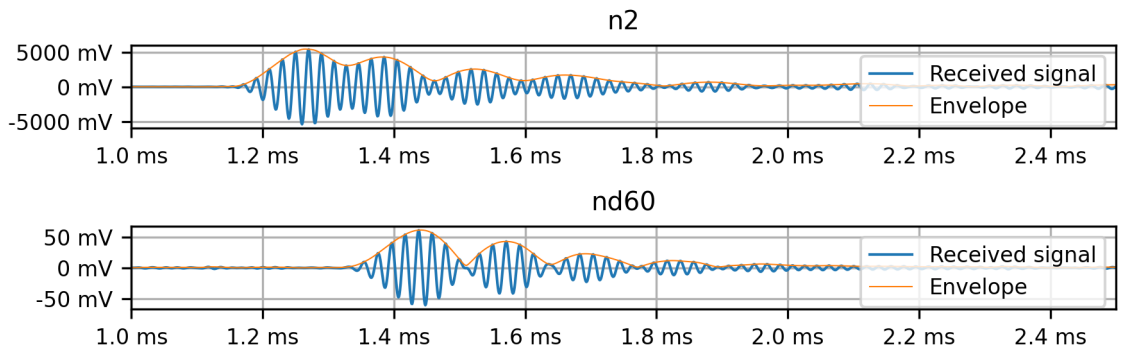

Figure 5.2: Comparison of echoes in Tx6 for nitrogen (upper) and the nd60 (lower) gas mixture. The envelope is calculated using hilbert-transforms.

By changing the number of cycles on the signal generator and observing the wavelets, echoes were found for all transducers except for tx4. However, tx4 could not give results in carbon dioxide due to the large sound absorption as seen in fig. C.4.

The low-frequency transducers (tx1, tx2, tx3) was largely disrupted by echoes and other effects. This could be explained by resonance in the surrounding materials having lower resonance frequencies.

5.1.2 Conclusion of Signal Quality

Due to the low-quality signals from the transducers with low frequency (tx1, tx2, tx3), these were chosen to not be included in the modeling later.

Tx5 also had insufficient quality of the response and was not included for the modeling.

Therefore, only the transducers tx4, tx6, and tx7 was included for further analysis, whereas only tx6 gave signals in carbon dioxide.

5.2 Comparison with Theoretical Model

When comparing the theoretical model with the experimental results it was chosen to look at the attenuation factor (α) and the speed of sound (c). In these estimations, it was chosen to use relative errors since it is more intuitive. The mean relative error is calculated as:

$$\epsilon = \frac{1}{N} \sum_{i}^{N} \frac{|\hat{v}_i - v_i|}{v_i} \tag{5.2.1}$$

where N is the total number of samples, $\hat{v}_i$ is the estimated value (speed of sound or attenuation) and v_i is the theoretical value.

5.2.1 Attenuation

In fig. 5.3 below the attenuation is plotted for each transducer with the theoretical model. Note that for pure nitrogen the results fit very well since the model was calibrated in nitrogen.

α is calculated from the raw signals as:

$$\alpha = -\frac{1}{z} \ln \frac{A}{A_0} \tag{5.2.2}$$

For the higher concentrations of carbon dioxide the signal is not detectable in tx4 and tx6 due to noise. This causes the attenuation to flatten out.

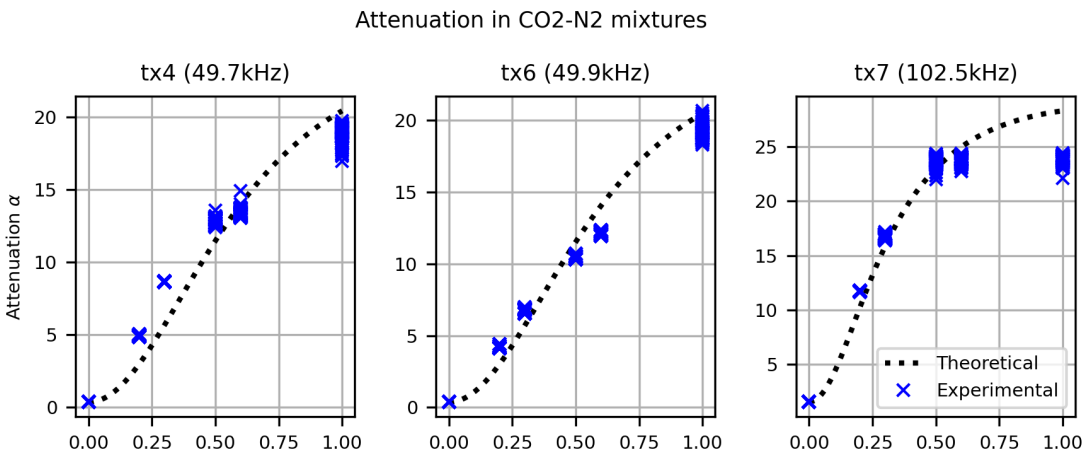

Figure 5.3: Attenuation in the carbon-dioxide nitrogen spectra for the chosen transducers. The dotted line shows the expected result from the theoretical model. The blue markers mark the experimental results. The y-axis shows the attenuation, α, and the carbon dioxide concentration is shown in the x-axis.

The relative amplitudes are shown in fig. 5.4 below. These give a good overview of how much the sound waves have been absorbed in the mixtures (10^0 is the original amplitude).

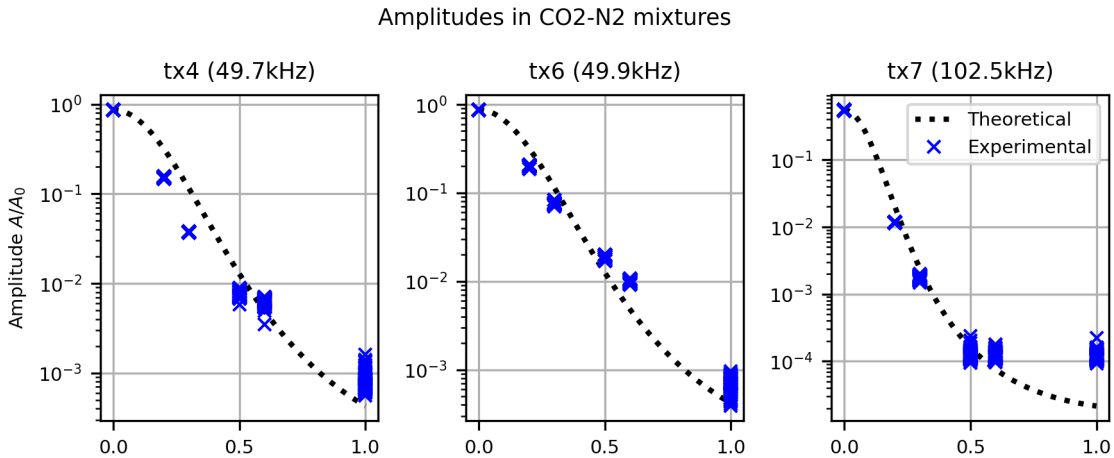

Figure 5.4: Amplitudes in the carbon-dioxide nitrogen spectra for the chosen transducers. The dotted line shows the expected result from the theoretical model. The blue markers mark the experimental results. The y-axis shows the relative amplitude, A/A_0, and the carbon dioxide concentration is shown in the x-axis.

The table 5.1 shows the mean relative error of the experimental results for attenuation, in average the error is 15.5% of the attenuation factor, α. Tx7 (100kHz) has lowest relative error at 7.6%. It can also be seen visually in fig. 5.3 that the experimental values fit the theoretical values well except for the measurements in CO_2.

Table 5.1: Mean relative errors for the experimental attenuations (α)

	Tx4	Tx6	Tx7	Avg
n2	0.0162	0.0171	0.0136	0.0156
nd20	0.6534	0.4127	0.1450	0.4037
nd30	0.5237	0.1818	0.0545	0.2533
nd50	0.1162	0.0881	0.0314	0.0786
nd60	0.0431	0.1357	0.0498	0.0762
co2	0.0785	0.0597	0.1601	0.0994
Avg	0.2385	0.1492	0.0757	0.1545

5.2.2 Speed of Sound

The results for speed of sound gave better results than for attenuation. For the combinations giving high SNR, the estimated speed of sound had an average relative error of less than 10%. In fig. 5.5 the estimated experimental values are plotted with the theoretical values. Note that for pure nitrogen the results fit very well since it was calibrated in nitrogen.

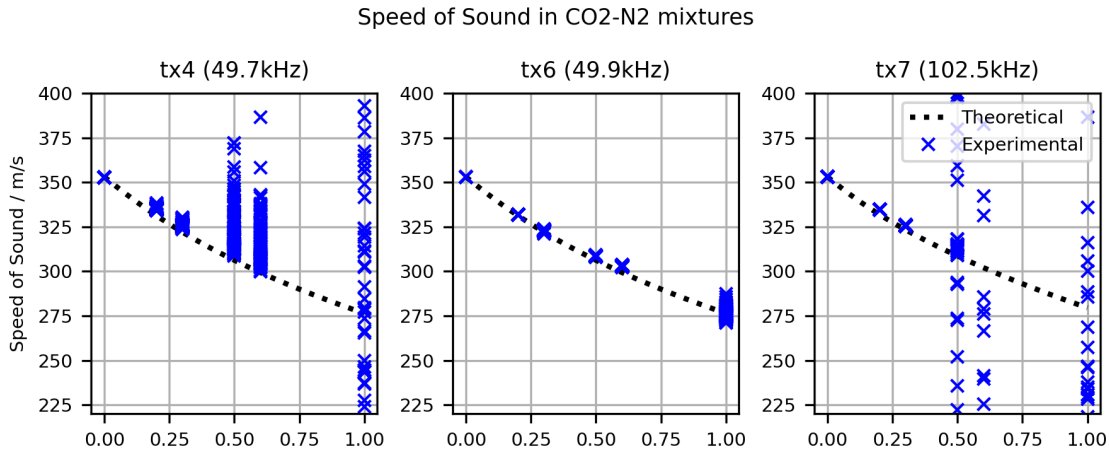

Figure 5.5: Speed of sound in the carbon-dioxide nitrogen spectra for the chosen transducers. The dotted line shows the expected result from the theoretical model. The blue markers are the experimental results using the envelope peak TDE estimator from section 4.4.4.

As expected the estimated speed of sound gives unconfident results in high concentrations of carbon dioxide for Tx4 and Tx7. This can be seen in table 5.2, tx6 has high SNR for all concentrations but seems to have increasing errors with the carbon dioxide concentration.

Table 5.2: Mean relative errors for the estimated speed of sound

	Tx4	Tx6	Tx7	Avg
n2	0.0009	0.0002	0.0004	0.0005
nd20	0.0119	0.0015	0.0083	0.0072
nd30	0.0123	0.0020	0.0072	0.0072
nd50	0.0619	0.0074	2.4619	0.8437
nd60	0.0633	0.0124	2.0708	0.7155
co2	1.8566	0.1482	21.0627	7.6892
Avg	0.3345	0.0286	4.2686	1.3294

The results in Tx6 gave best results when the SNR was sufficient high. For these measurements the average relative error was 0.13% on n2, nd20 and nd30. The error increases with the fraction of carbon dioxide, and the average error for Tx6 is at 2.6%.

5.3 Comparison of the Predictive Models

In table 5.3 all models are evaluated with the relevant metrics on the train and testing set. The MAE can be interpreted as the average error in the carbon dioxide

fraction, meaning that a MAE of 0.01 gives an average of ±1% error in the carbon dioxide fraction.

Table 5.3: Results from the various models

Model	Ref	Train		Test	
		R^2	MAE	R^2	MAE
SVR	4.5.2	0.969982	0.051814	0.961997	0.052518
SVR Calibrated	4.5.3	0.999583	0.004463	0.998997	0.006969
CNN	4.5.4	0.999289	0.006495	0.997974	0.009145

None of the models showed sign of overfitting. It was surprising how well the algorithms managed to explain the nd20 mixture correctly considering the complexity of the theoretical model. This shows that machine learning algorithms has a huge potential in gas sensing applications, and a good model can be created on a subset of the relevant gas mixtures.

The calibrated SVM proved to be the best suited model with an MAE of 0.006969 for the test set. This is the same as an error of ±0.697% in the carbon dioxide fraction estimates.

5.3.1 Final Model

The calibrated support vector machine proved to be the best suited model. In table 5.4 error estimates for all gases are shown. For the nd20 gas only test results are available since these have not been used for training. Since the error decreases with the fraction of carbon dioxide it can be assumed that in mixtures with carbon dioxide fraction below 20% the absolute errors should be less than 0.5%.

Table 5.4: Error estimations as percentage for the final predictive model

Gas mixture	% CO_2	Train		Test	
		MAE /%	RMSE /%	MAE /%	RMSE /%
n2	0	0.066	0.082	0.056	0.070
nd20	20			0.313	0.392
nd30	30	0.185	0.216	0.723	0.730
nd50	50	0.626	0.750	1.427	1.454
nd60	60	0.705	1.020	1.579	1.620
co2	100	0.657	0.812	0.998	1.135
Overall		0.446	0.678	0.697	0.920

5.3.2 Comparison with Related Work

Compared to the model proposed by Zhao, Lou, and Xu in [30] the model provided in this work does better in predicting the carbon dioxide fraction. While their model had RMSE ranging from 3.1% up to 7.7% the model provided here has RMSE ranging from 0.39% to 1.6% (invalidating the results in nitrogen due to calibration).

While Zhao, Lou, and Xu used curve fitting to find the correct parameters (which requires knowledge of the physical properties of the gas components), the predictive model proposed here only relies on calibration in nitrogen and the experimental data already needed for model validation. This shows that machine learning has a huge potential in gas sensing for predicting gas concentrations, and it does not require knowledge of the physical properties of the relevant gas as long as experimental data can be obtained.

5.4 Problems and Uncertainties with Experimental Testing

During the experiments some problems were revealed as potential causes of uncertainty, noise or even incorrect data.

The first experiments were done on damaged coaxial cables which gave varying results. This was corrected by changing to newer cables. After changing the cables, it was not found evidence of this happening in the results presented here.

Some transducer fittings were found to leak gas. This was most notable in the fitting for tx6. Since the experiments show good compliance with theory and the predictive model, this is not assumed to have given any significant errors in the experiments. But for further work the leakage should be resolved.

6. Conclusion

6.1 Summary

In this work there was a wide focus on the theoretical fundamentation causing a non-linear relationship in the attenuation and speed of sound in mixtures of carbon dioxide and nitrogen. Based on the theories of relaxation a model was developed in the python programming language which models any mixture of nitrogen and carbon dioxide and predicts speed of sound and attenuation for any given frequency.

Using a custom-made test rig, experimental data was obtained for a set of transducers with frequencies ranging from 25 to 100 kHz together with a set of gas mixtures in the CO_2—N_2 spectrum. The results showed that the theoretical model has good assumptions which fits the experimental results well. Even tough, there are some offsets between predicted and experimental attenuation. In average the relative error for the attenuation factor, α, was 15.5% and 7.57% for the transducer tx7 which gave best results.

The predicted and experimental speed of sound shows a better fit than for attenuation. For the transducer giving signal in all gas mixtures, Tx6 (49.9kHz), the average relative error for the speed of sound was 2.86%.

For solving the inverse problem of predicting the gas mixture the experimental data was used for training a machine learning model. The test set consisted of a series of samples from the first experimental run and all data from the gas mixture containing 80%N_2 and 20%CO_2. Using the remaining data for training, a set of machine learning models were tested and evaluated. The final model, using a Support Vector Machine for regression, achieved a mean error (MAE) of 0.697% for the test set, meaning that the predicted concentration is in average 0.697% offset from the actual concentration (not relative). This is an improvement compared to the related work using transducers for gas sensing, where the errors were seen larger than 2.4% absolute error in the CO_2 fraction.

6.2 Further Work

The method described here gave promising results, but there are some improvements which could improve the concept of using transducers for gas sensing.

6.2.1 Improving the Experimental Data

Improving the test rig for further analysis can give beneficial results. To summarize, the following bullets are the suggested further work for improved results:

- Ensure proper sealing of the chamber.

- Improve transducer fittings to avoid potential echoes.
- Improve pre-amplification to allow higher voltages on the transducers to obtain signals in carbon dioxide.
- Usage of gas-mixers to allow experimenting with more gas mixtures.
- Find more usable transducers which can replace those that were not used due to bad quality.

These improvements are expected to give higher quality of the data and by having more gas mixtures the accuracy of the model should be improved.

6.2.2 Improving the Models

The predictive models gave satisfactory results, but it is possible they can be improved to give better results.

Improving and testing more preprocessing methods can give beneficial results. For example by using wavelet decomposition (similarly as it was done in [29]) or looking at the signals in a frequency domain other useful features might be extracted from the signals.

6.2.3 Extended Analysis

The work described here only included a limited set of gas mixtures and transducer frequencies. Using more gases and gas mixers, a wider spectra with multiple components can be used to create better predictive models.

Finding more usable transducers which allows having more frequencies, or even allowing frequency sweeping, could have a large potential for predictive models as stated in [16, 17].

Bibliography

[1] S. Feng, F. Farha, Q. Li, Y. Wan, Y. Xu, T. Zhang, and H. Ning, "Review on Smart Gas Sensing Technology," *Sensors*, vol. 19, no. 17, 2019, ISSN: 1424-8220. DOI: 10.3390/s19173760.

[2] W. H. Assembly, "Health, environment and climate change: Report by the director-general," 2018. [Online]. Available: https://apps.who.int/iris/handle/10665/276332.

[3] W.-T. Tsai, "The decomposition products of sulfur hexafluoride (sf6): Reviews of environmental and health risk analysis," *Journal of Fluorine Chemistry*, vol. 128, no. 11, pp. 1345–1352, 2007, ISSN: 0022-1139. DOI: https://doi.org/10.1016/j.jfluchem.2007.06.008.

[4] R. Younes, S. Lakkis, Y. Alayli, and M. Sawan, "Review Of Recent Trends in Gas Sensing Technologies and their Miniaturization Potential," *Sensor Review*, vol. 34, Jan. 2014. DOI: 10.1108/SR-11-2012-724.

[5] M. Huber and A. Harvey, *Viscosity of Gases*, en, 92nd Ed. CRC-Press, Boca Raton, FL, Jun. 2011. [Online]. Available: https://tsapps.nist.gov/publication/get_pdf.cfm?pub_id=907539.

[6] M. Huber, *Thermal Conductivity of Gases*, en. CRC Handbook of Chemistry and Physics, CRC Press, Boca Raton, FL, Jul. 2019. [Online]. Available: https://tsapps.nist.gov/publication/get_pdf.cfm?pub_id=926438.

[7] *Pubchem compound summary for cid 947, nitrogen.* May 2021. [Online]. Available: https://pubchem.ncbi.nlm.nih.gov/compound/Nitrogen.

[8] *Pubchem compound summary for cid 280, carbon dioxide.* May 2021. [Online]. Available: https://pubchem.ncbi.nlm.nih.gov/compound/Carbon-dioxide.

[9] M. J. S. Lowe, "Ultrasonics," in *Encyclopedia of Vibration*, S. Braun, Ed., Oxford: Elsevier, 2001, pp. 1437–1441, ISBN: 978-0-12-227085-7. DOI: 10.1006/rwvb.2001.0143.

[10] T. G. Leighton, "What is ultrasound?" *Progress in Biophysics and Molecular Biology*, vol. 93, no. 1, pp. 3–83, 2007, Effects of ultrasound and infrasound relevant to human health, ISSN: 0079-6107. DOI: 10.1016/j.pbiomolbio.2006.07.026.

[11] P.-E. Martinsson and J. Delsing, "Ultrasonic measurements of molecular relaxation in ethane and carbon monoxide," vol. 1, Nov. 2002, pp. 511–516, ISBN: 0-7803-7582-3. DOI: 10.1109/ULTSYM.2002.1193454.

[12] P. J. Mohr, D. B. Newell, and B. N. Taylor, "CODATA recommended values of the fundamental physical constants: 2014," *Rev. Mod. Phys.*, vol. 88, p. 035 009, 3 Sep. 2016. DOI: 10.1103/RevModPhys.88.035009.

[13] A. G. Petculescu and R. M. Lueptow, "Synthesizing Primary Molecular Relaxation Processes in Excitable Gases Using a Two-Frequency Reconstructive Algorithm," *Phys. Rev. Lett.*, vol. 94, 23 Jun. 2005. DOI: 10.1103/PhysRevLett.94.238301.

[14] K. F. Herzfeld and T. A. Litovitz, *Absorption and Dispersion of Ultrasonic Waves*, H. S. W. Massey and K. A. Brueckner, Eds. Academic Press, 1959, ISBN: 9781483275703. [Online]. Available: https://www.elsevier.com/books/absorption-and-dispersion-of-ultrasonic-waves/herzfeld/978-1-4832-3057-3.

[15] K.-S. Zhang, S. Wang, M. Zhu, Y. Ding, and Y. Hu, "Decoupling multimode vibrational relaxations in multi-component gas mixtures: Analysis of sound relaxational absorption spectra," *Chinese Physics B*, vol. 22, no. 1, p. 014 305, Jan. 2013. DOI: 10.1088/1674-1056/22/1/014305.

[16] A. Petculescu and P. L. D. Lueptow Richard, "Quantitative Acoustic Relaxational Spectroscopy for real-time monitoring of natural gas: A perspective on its potential," *Sensors and Actuators B: Chemical*, vol. 169, pp. 121–127, 2012. DOI: 10.1016/j.snb.2012.03.086.

[17] X. Zhang, S. Wang, and M. Zhu, "Locating the inflection point of frequency-dependent velocity dispersion by acoustic relaxation to identify gas mixtures," *Measurement Science and Technology*, vol. 31, no. 11, p. 115 001, Sep. 2020. DOI: 10.1088/1361-6501/ab9375.

[18] M. Zhu, T. Liu, S. Wang, and K. Zhang, "Capturing molecular multimode relaxation processes in excitable gases based on decomposition of acoustic relaxation spectra," *Measurement Science and Technology*, vol. 28, Jul. 2017. DOI: 10.1088/1361-6501/aa544d.

[19] W. Liu Tingting, Z. Shu, and Ming, "Predicting acoustic relaxation absorption in gas mixtures for extraction of composition relaxation contributions," *Proceedings of the Royal Society A*, Dec. 2017. DOI: 10.1098/rspa.2017.0496.

[20] W. J. Witteman, "Vibrational Relaxation in Carbon Dioxide," *The Journal of Chemical Physics*, vol. 35, no. 1, pp. 1–9, 1961. DOI: 10.1063/1.1731873.

[21] C. M. Bishop, *Pattern Recognition and Machine Learning (Information Science and Statistics)*. Berlin, Heidelberg: Springer-Verlag, 2006, ISBN: 0387310738.

[22] N. H. Sweilam, A. A. Tharwat, and N. K. Abdel Moniem, "Support vector machine for diagnosis cancer disease: A comparative study," *Egyptian Informatics Journal*, vol. 11, no. 2, pp. 81–92, 2010, ISSN: 1110-8665. DOI: https://doi.org/10.1016/j.eij.2010.10.005.

[23] C.-C. Chang and C.-J. Lin, "LIBSVM: A Library for Support Vector Machines," *ACM Trans. Intell. Syst. Technol.*, vol. 2, no. 3, May 2011, ISSN: 2157-6904. DOI: 10.1145/1961189.1961199.

[24] I. Goodfellow, Y. Bengio, and A. Courville, *Deep Learning*. MIT Press, 2016, http://www.deeplearningbook.org.

[25] H. Toda and T. Kobayakawa, "High-speed gas concentration measurement using ultrasound," *Sensors and Actuators A: Physical*, vol. 144, pp. 1–6, May 2008. DOI: 10.1016/j.sna.2007.12.025.

[26] A. Petculescu, B. Hall, R. Fraenzle, S. Phillips, and R. M. Lueptow, "A prototype acoustic gas sensor based on attenuation," *The Journal of the Acoustical Society of America*, vol. 120, no. 4, pp. 1779–1782, 2006. DOI: 10.1121/1.2336758.

[27] Y. Hu, S. Wang, M. Zhu, K. Zhang, T. Liu, and D. Xu, "Acoustic absorption spectral peak location for gas detection," *Sensors and Actuators B: Chemical*, vol. 203, pp. 1–8, 2014, ISSN: 0925-4005. DOI: https://doi.org/10.1016/j.snb.2014.05.091.

[28] K.-S. Zhang, S. Wang, M. Zhu, and Y. Ding, "Algorithm for capturing primary relaxation processes in excitable gases by two-frequency acoustic measurements," *Measurement Science and Technology*, vol. 24, no. 5, p. 055 002, Mar. 2013. DOI: 10.1088/0957-0233/24/5/055002.

[29] Y. Jia, B. Yu, M. Du, and X. Wang, "Gas Composition Recognition Based on Analyzing Acoustic Relaxation Absorption Spectra: Wavelet Decomposition and Support Vector Machine Classifier," in *Proceedings of the 2018 2nd International Conference on Electrical Engineering and Automation (ICEEA 2018)*, Atlantis Press, Mar. 2018. DOI: 10.2991/iceea-18.2018.28.

[30] W. Zhao, W. Lou, and Y. Xu, "Concentration measurement of carbon dioxide based on ultrasonic principle," *Measurement: Sensors*, vol. 15, p. 100 040, 2021, ISSN: 2665-9174. DOI: https://doi.org/10.1016/j.measen.2021.100040.

[31] S. Sherrit, H. D. Wiederick, and B. K. Mukherjee, "Accurate equivalent circuits for unloaded piezoelectric resonators," in *1997 IEEE Ultrasonics Symposium Proceedings. An International Symposium (Cat. No.97CH36118)*, vol. 2, Oct. 1997, pp. 931–935. DOI: 10.1109/ULTSYM.1997.661733.

[32] I. The MathWorks, *Signal Processing Toolbox™User's Guide*, R2020b, The MathWorks, Inc, 2020. [Online]. Available: https://mathworks.com/help/signal/.

[33] F. Gustafsson, "Determining the initial states in forward-backward filtering," *IEEE Transactions on Signal Processing*, vol. 44, no. 4, pp. 988–992, Apr. 1996, ISSN: 1941-0476. DOI: 10.1109/78.492552.

[34] C. Bentz, L. Baudzus, and P. Krummrich, "Signal to Noise Ratio (SNR) Enhancement Comparison of Impulse-, Coding- and Novel Linear-Frequency-Chirp-Based Optical Time Domain Reflectometry (OTDR) for Passive Optical Network (PON) Monitoring Based on Unique Combinations of Wavelength Selective Mirrors," *Photonics*, vol. 1, pp. 33–46, Mar. 2014. DOI: 10.3390/photonics1010033.

[35] W. Gragido, J. Pirc, N. Selby, and D. Molina, "Chapter 4 - signal-to-noise ratio," W. Gragido, J. Pirc, N. Selby, and D. Molina, Eds., pp. 45–55, 2013. DOI: https://doi.org/10.1016/B978-1-59-749740-4.00004-6.

[36] A. V. Oppenheim and R. W. Schafer, "Discrete-Time Signals and Systems," in *Discrete-Time Signal Processing*, Third. USA: Prentice Hall Press, 2009, ch. 2, pp. 9–98, ISBN: 0131988425.

[37] A. Hero, H. Messer, J. Goldberg, D. J. Thomson, M. G. Amin, G. Giannakis, A. Swami, J. K. Tugnait, A. Nehorai, A. L. Swindlehurst, J. . Cardoso, L. Tong, and J. Krolik, "Highlights of statistical signal and array processing," *IEEE Signal Processing Magazine*, vol. 15, no. 5, pp. 21–64, Sep. 1998, ISSN: 1558-0792. DOI: 10.1109/79.708539.

[38] T. Kurbiel and S. Khaleghian, "Training of Deep Neural Networks based on Distance Measures using RMSProp," *CoRR*, vol. abs/1708.01911, Aug. 2017. arXiv: 1708.01911. [Online]. Available: http://arxiv.org/abs/1708.01911.

A. Data Acquisition Protocol

This protocol is to be followed when doing measurements in the test rig.

A.1 Objectives

- Measure the attenuation and velocity over a frequency range using provided transducers (25kHz-100kHz)
- The tests should result in .csv files containing one array for time, transmitted signal and received signal.

Folder structure should be like:

```
data/tx<id>/<gas_id>/run<n>/run<n>_<m>.csv
```

where `n` is the run number (each run consists of 32 measurements) and `m` is the measurement number. The transducers are identified by `tx<id>` and the gas is identified by `<gas_id>`.

In each transducer folder `data/tx<id>` a file named parameters.txt should describe the parameters used for the transducer. Eg:

```
freq: 102.5kHz
vpp: 0.800V (x6 trafo)
n_cycles: 7
pre-amp: 100x
```

A.2 Determination of test parameters

Test parameters are determined based on tests in nitrogen. Optimal frequency is set as the frequency giving the highest amplitude of the received signal. Voltage (vpp) from the generator is set as near the transducers max voltage as possible.

Number of cycles should be set such that the bursts have as high amplitude as possible and giving signals which are not disrupted by echoes or off-phase responses.

Pre-amp setting of the microphone is set to 100x if the signal does not overload in nitrogen, if it does it is set to 10x.

A.3 Setup

Oscilloscope:

- Set window div to 500us/div
- Number of samples should be set such that the sample frequency is near 1 MS/s, at 500us/div the setting should be 6kS.

- Configure channels (no Auto range, set range as low as possible for the given gas without overrange)
  - A: Frequency generator burst (sig-out on the amplifier)
  - B: Microphone
- Trigger setting
  - Trig on channel A,
  - Set pre-sample to 10%
  - Trigger to rising, at 100mV

Frequency Generator:

1. Set to continuous mode:
   - Set amplitude from parameters.txt
   - Set frequency from parameters.txt
2. Set to burst mode:
   - Set n_cycles to the value from parameters.txt

Power Supply:

- Set voltage to 9V
- Current limit to 0.2A
- If OC, turn off voltage, plug out BNC cables, turn on voltage, and plug cables in again

Microphone Pre-Amplifier:

- Set Pre-amp to the value in parameters.txt
- Linear convolve

A.4 Procedure

1. Fill the gas chamber with the target gas:
   - Open outlet valve
   - Attach the regulator and the tubes
   - Set regulator to 1L/s
   - Fill for at least 4 minutes
   - Close the main valve
   - Close outlet valve
   - Wait for 4 minutes to let the gas settle
2. Take measurements:
   - Set channel B voltage range to as low as possible without overrange.
   - The PicoScope software should have buffered at least 32 samples before saving
   - Ensure that there are no errors, overranges, or outer disturbances amongst the 32 samples
   - Save the samples as csv files with the folder `data/tx<id>/<gas_id>/run<n>`
   - Repeat for at least 4 runs

B. Transducer Characteristics

The following are the results from characterization with the impedance analyzer, the quality of the measurements are unknown but expected to be high.

Frequency are taken from the respective transducers' data sheet, and the voltages are the maximum peak to peak ratings.

B.1 Equivalent Circuit:

```
  ----C0----
-|          |-
  -L1-C1-R1-
```

B.2 Characteristics

Id	Frequency [kHz]	Vpp [V]	C0 [F]	C1 [F]	R1 [Ohm]	L1 [H]
Tx1	25.0 ± 1.0kHz	56	2.497e-009	2.935e-010	6.716e+002	1.318e-001
Tx2	32.8 ± 1.0kHz	56	2.300e-009	1.250e-010	4.627e+002	1.861e-001
Tx3	40.0 ± 1.0kHz	56	2.616e-009	1.440e-010	7.647e+002	1.148e-001
Tx4	49.5	N/A	4.949e-010	2.020e-011	1.920e+003	5.003e-001
Tx5	60.0	N/A	7.783e-010	1.233e-010	2.111e+002	5.650e-002
Tx6	50.0	1000	1.058e-009	3.538e-010	1.540e+002	2.352e-002
Tx7	100.0 ± 8.0kHz	600	6.325e-010	1.198e-010	5.112e+002	2.202e-002

C. Sample Signal Responses

C.1 Tx1

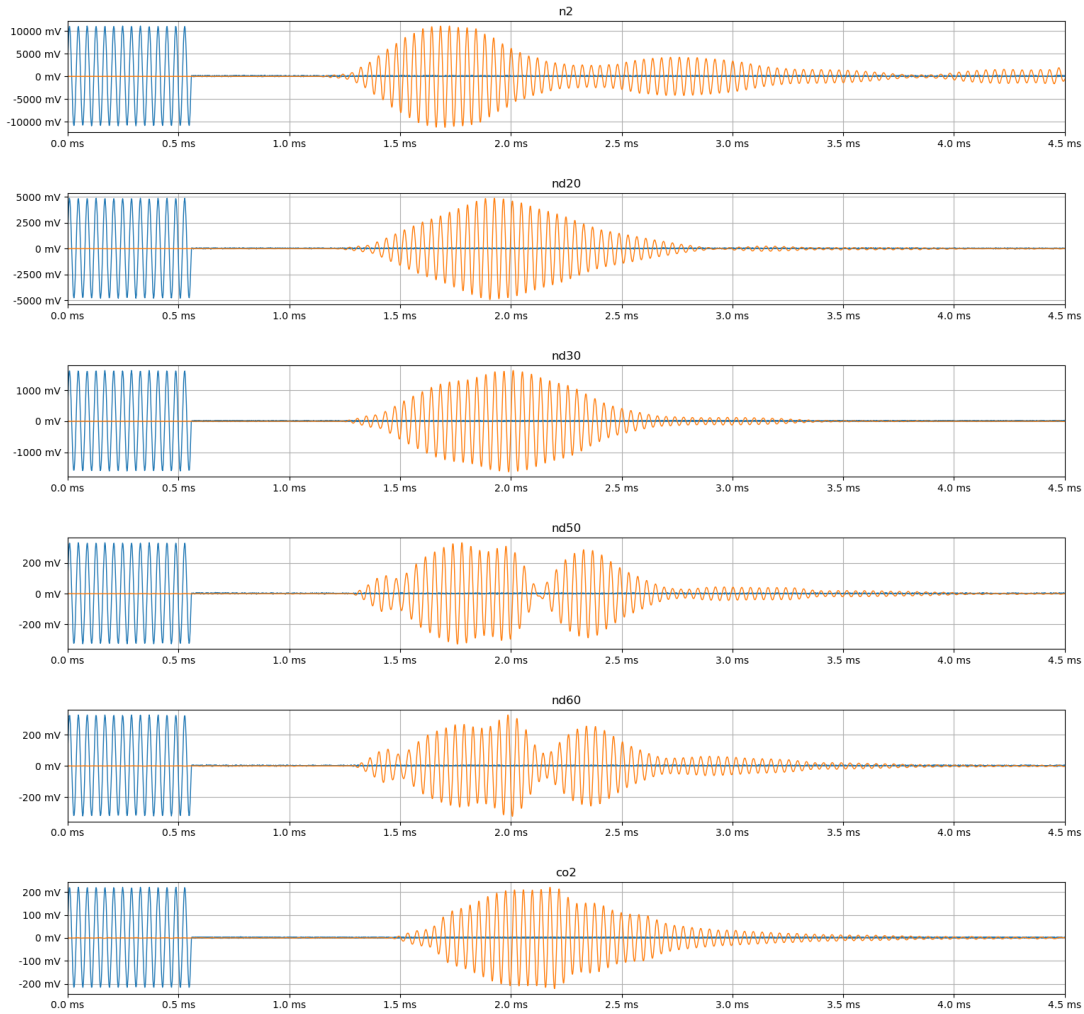

Figure C.1: Filtered signal samples from Tx1 in the nitrogen/carbon-dioxide spectrum. The blue signal is the generated burst normalized to the maximum of the received signal for illustration purposes, the orange signal is the received signal A. Compositions of the gas mixtures can be found in table 4.3.

C.2 Tx2

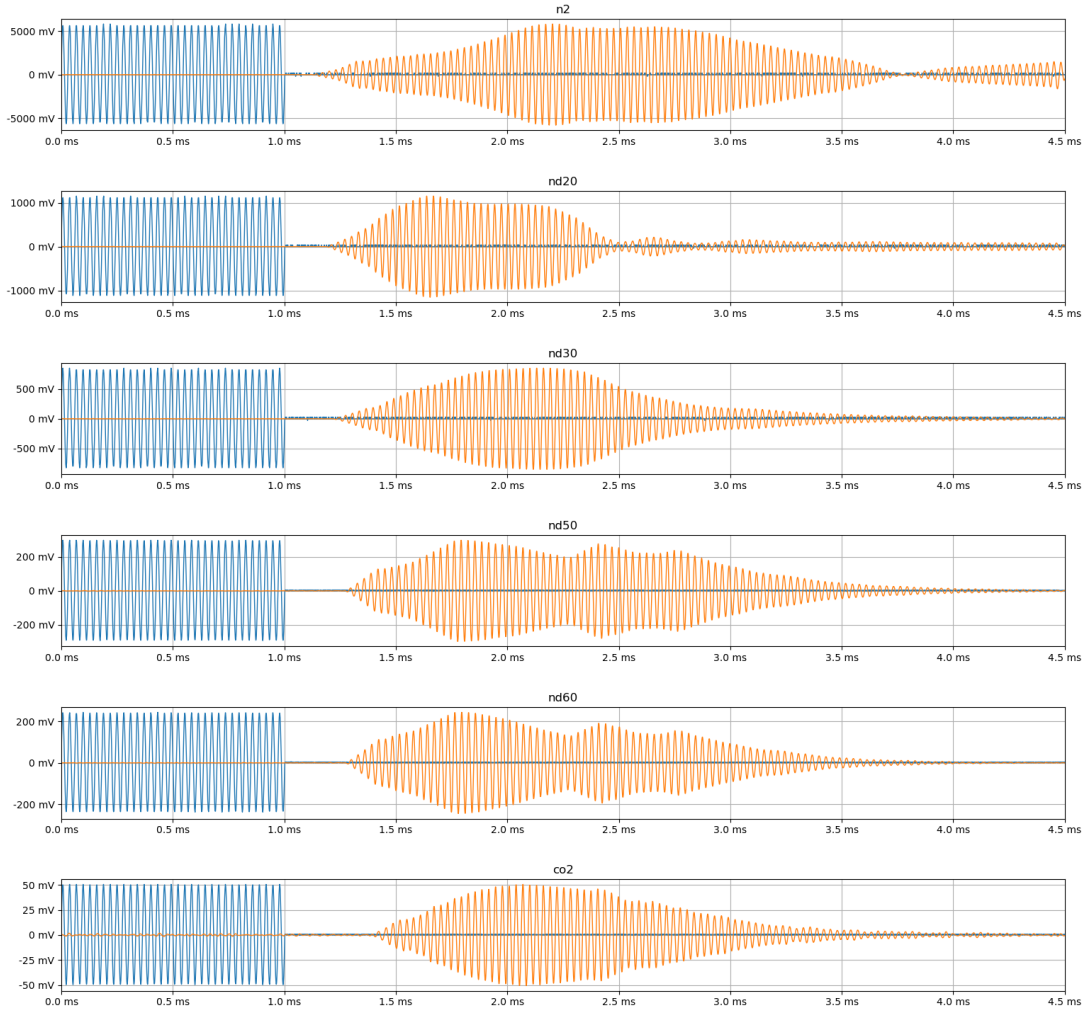

Figure C.2: Filtered signal samples from Tx2 in the nitrogen/carbon-dioxide spectrum. The blue signal is the generated burst normalized to the maximum of the received signal for illustration purposes, the orange signal is the received signal A. Compositions of the gas mixtures can be found in table 4.3.

C.3 Tx3

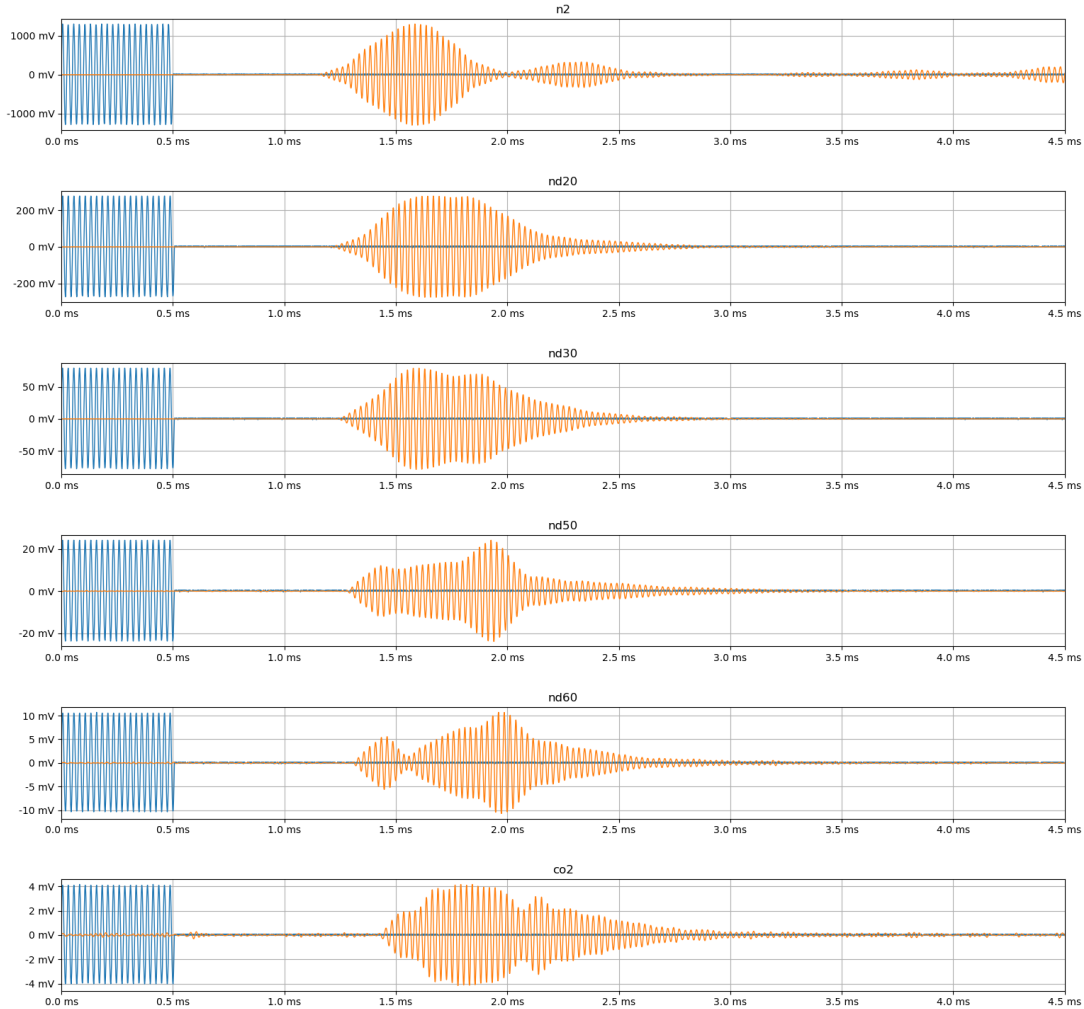

Figure C.3: Filtered signal samples from Tx3 in the nitrogen/carbon-dioxide spectrum. The blue signal is the generated burst normalized to the maximum of the received signal for illustration purposes, the orange signal is the received signal A. Compositions of the gas mixtures can be found in table 4.3.

C.4 Tx4

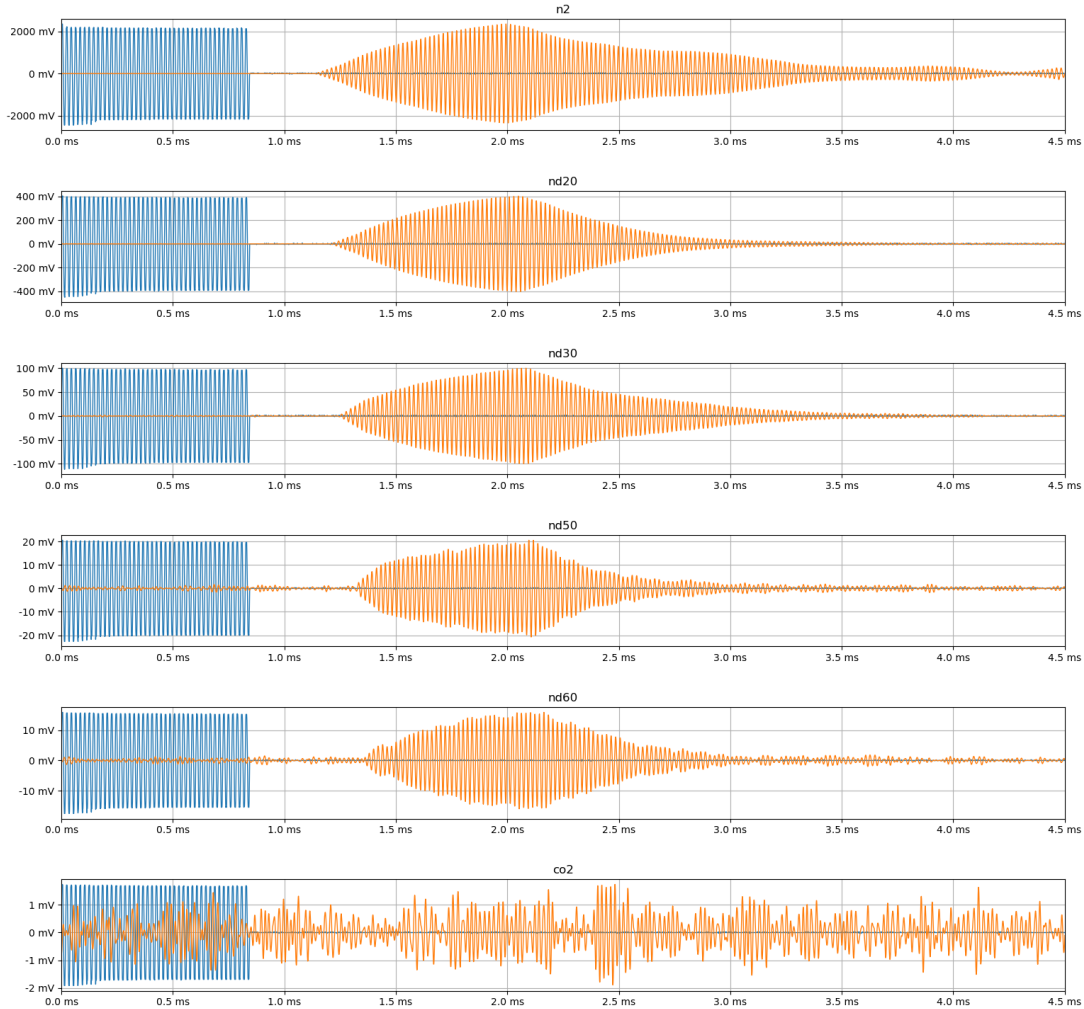

Figure C.4: Filtered signal samples from Tx4 in the nitrogen/carbon-dioxide spectrum. The blue signal is the generated burst normalized to the maximum of the received signal for illustration purposes, the orange signal is the received signal A. Compositions of the gas mixtures can be found in table 4.3.

C.5 Tx5

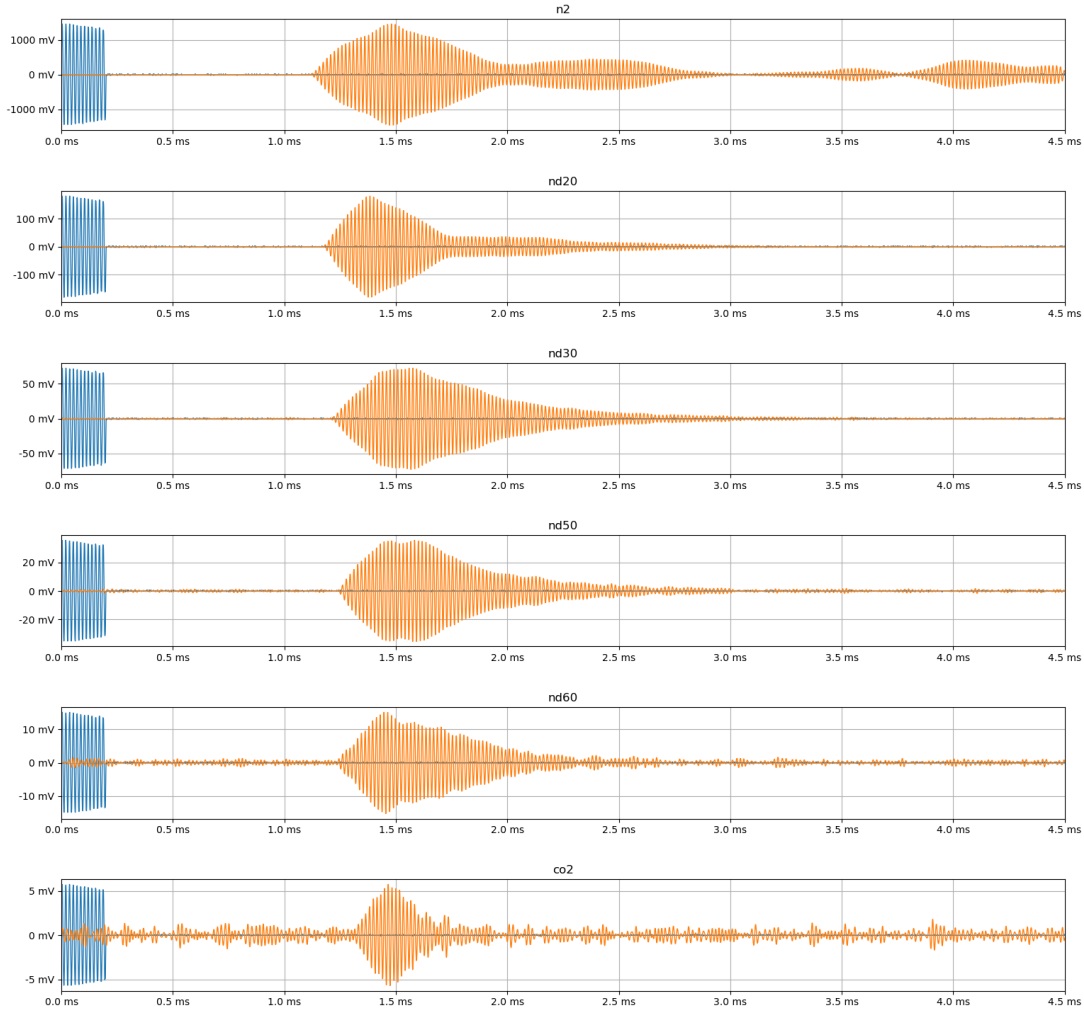

Figure C.5: Filtered signal samples from Tx5 in the nitrogen/carbon-dioxide spectrum. The blue signal is the generated burst normalized to the maximum of the received signal for illustration purposes, the orange signal is the received signal A. Compositions of the gas mixtures can be found in table 4.3.

C.6 Tx6

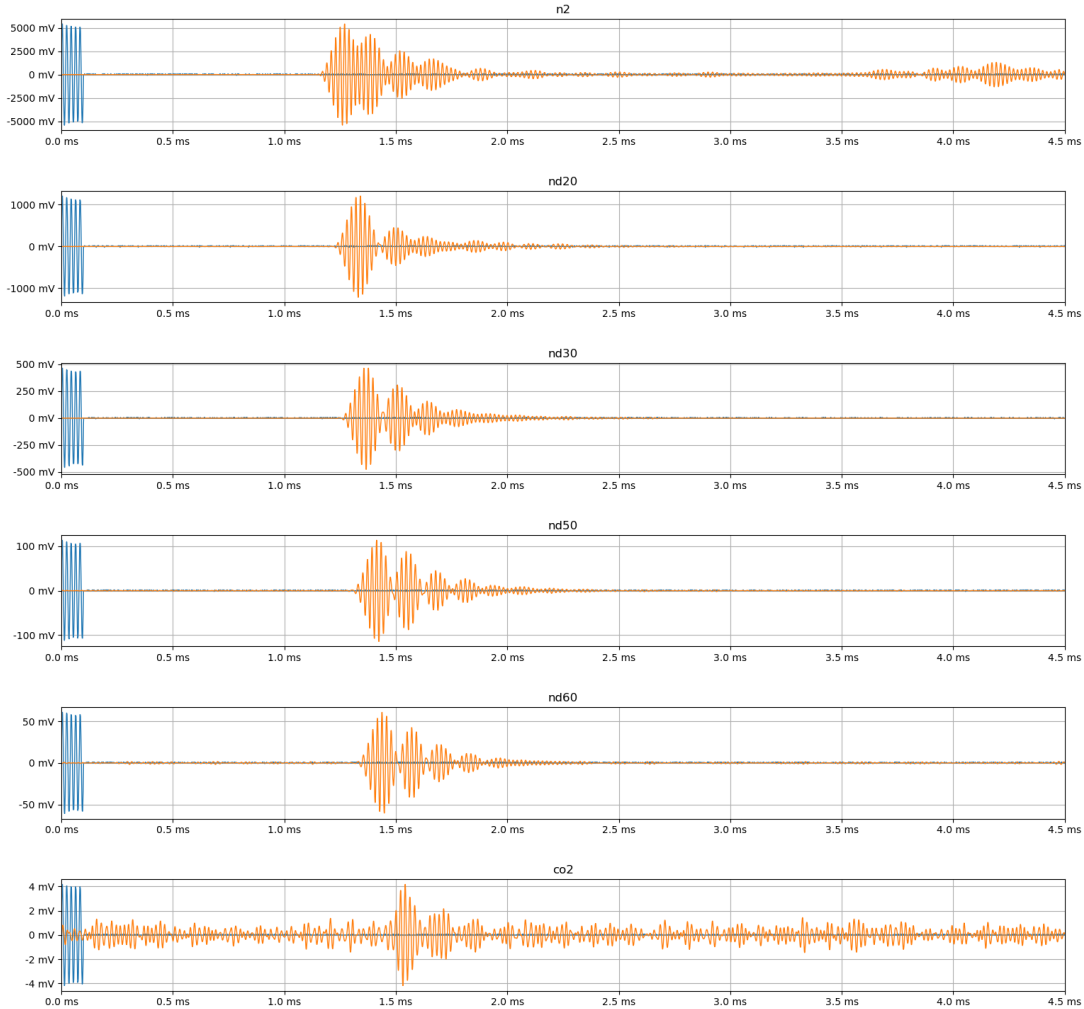

Figure C.6: Filtered signal samples from Tx6 in the nitrogen/carbon-dioxide spectrum. The blue signal is the generated burst normalized to the maximum of the received signal for illustration purposes, the orange signal is the received signal A. Compositions of the gas mixtures can be found in table 4.3.

C.7 Tx7

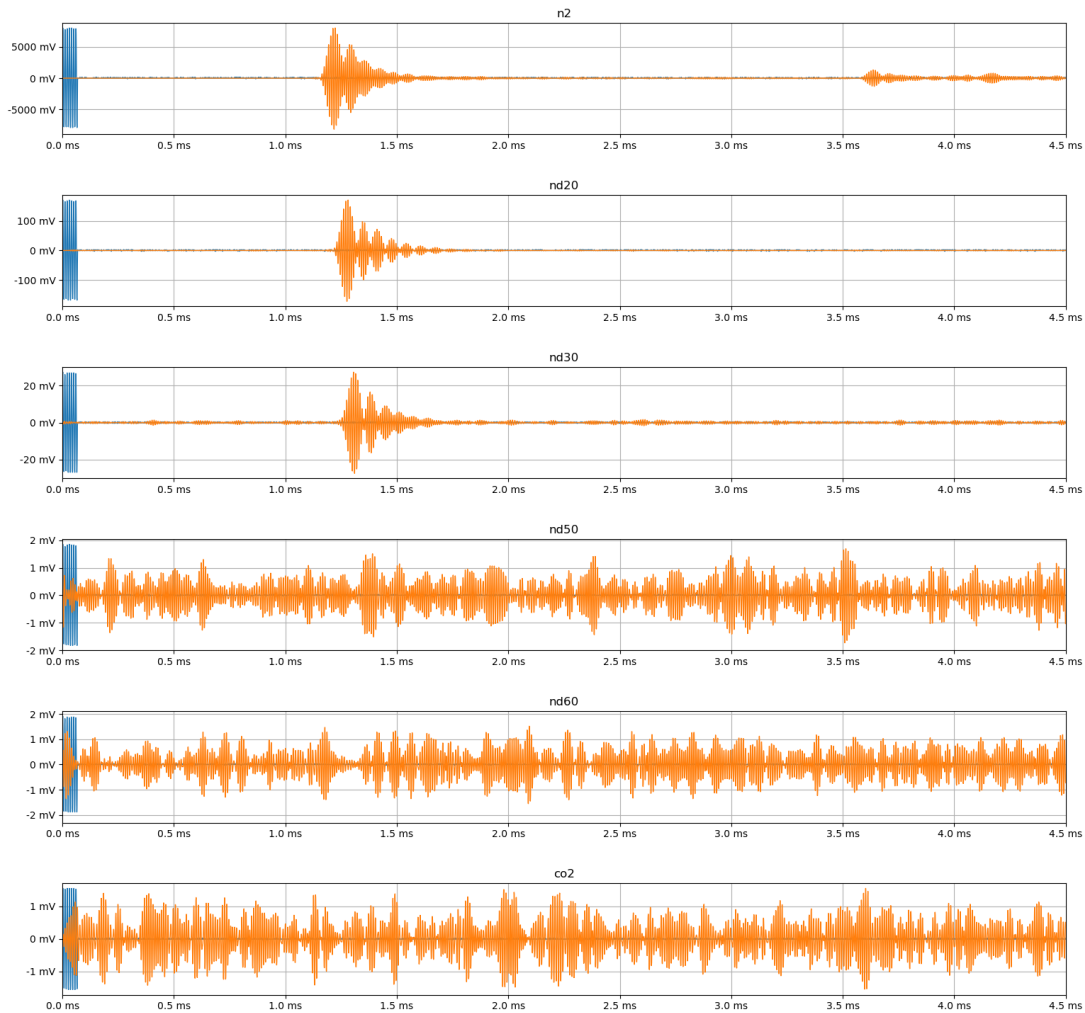

Figure C.7: Filtered signal samples from Tx7 in the nitrogen/carbon-dioxide spectrum. The blue signal is the generated burst normalized to the maximum of the received signal for illustration purposes, the orange signal is the received signal A. Compositions of the gas mixtures can be found in table 4.3.

Norges miljø- og biovitenskapelige universitet
Noregs miljø- og biovitskapelege universitet
Norwegian University of Life Sciences

Postboks 5003
NO-1432 Ås
Norway